Mon. Not. R. Astron. Soc. **000**, 1–15 (XXXX) Printed 19 May 2014 (MN LATEX style file v2.2)

# GRB 051008: A long, spectrally-hard dust-obscured GRB in a Lyman-Break Galaxy at $z \approx 2.8$*

A. A. Volnova,[1⋆] A. S. Pozanenko,[1]† J. Gorosabel,[2] D. A. Perley,[3,4] D. D. Frederiks,[5] D. A. Kann,[6,7] V. V. Rumyantsev,[8] V. V. Biryukov,[8,9] O. Burkhonov,[10] A. J. Castro-Tirado,[2] P. Ferrero,[11,12] S. V. Golenetskii,[5] S. Klose,[6] V. M. Loznikov,[1] P. Yu. Minaev,[1] B. Stecklum,[6] D. S. Svinkin,[5] A. E. Tsvetkova,[5] A. de Ugarte Postigo,[2,13] and M. V. Ulanov[5]

[1]*Space Research Institute, 84/32 Profsoyuznaya Street, Moscow 117997, Russia*
[2]*Instituto de Astrofísica de Andalucía del Consejo Superior de Investigaciones Cientificas (IAA-CSIC), Camino Bajo de Huetor 50, E-18080 Granada, Spain*
[3]*Department of Astronomy, California Institute of Technology, MC 249-17, 1200 East California Blvd., Pasadena, CA 91125, USA*
[4]*Hubble Fellow*
[5]*Ioffe Physical-Technical Institute, Politekhnicheskaya 26, St. Petersburg 194021, Russia*
[6]*Thüringer Landessternwarte Tautenburg,Sternwarte 5, 07778 Tautenburg, Germany*
[7]*Max-Planck-Institut für extraterrestrische Physik, Giessenbachstraße 1, 85748 Garching, Germany*
[8]*Crimean Astrophysical Observatory, Taras Shevchenko National University of Kyiv, Nauchny, Crimea 98409, Ukraine*
[9]*Crimean Laboratory of the Sternberg Astronomical Institute, Nauchny, Crimea 98409, Ukraine*
[10]*Institute of Astronomy, Academy of Sciences of Uzbekistan, Tashkent, Uzbekistan*
[11]*Instituto de Astrofisica de Canarias (IAC), 38200 La Laguna, Tenerife, Spain*
[12]*Departamento de Astrofisica, Universidad de La Laguna (ULL), 38205 La Laguna, Tenerife, Spain*
[13]*Dark Cosmology Centre, Niels Bohr Institute, University of Copenhagen, Juliane Maries Vej 30, 2100 Copenhagen, Denmark*
∗*Based on observations made with the Nordic Optical Telescope, operated on the island of La Palma jointly by Denmark, Finland, Iceland, Norway, and Sweden, in the Spanish Observatorio del Roque de los Muchachos of the Instituto de Astrofisica de Canarias.*

arXiv:1405.4139v1 [astro-ph.HE] 16 May 2014

Accepted XXXX. Received XXXX.

**ABSTRACT**

We present observations of the dark Gamma-Ray Burst GRB 051008 provided by *Swift*/BAT, *Swift*/XRT, Konus-*WIND*, *INTEGRAL*/SPI-ACS in the high-energy domain and the Shajn, *Swift*/UVOT, Tautenburg, NOT, Gemini and Keck I telescopes in the optical and near-infrared bands. The burst was detected only in gamma- and X-rays and neither a prompt optical nor a radio afterglow were detected down to deep limits. We identified the host galaxy of the burst, which is a typical Lyman-break Galaxy (LBG) with $R$-magnitude of $24\overset{\mathrm{m}}{.}06 \pm 0\overset{\mathrm{m}}{.}10$. A redshift of the galaxy of $z = 2.77^{+0.15}_{-0.20}$ is measured photometrically due to the presence of a clear, strong Lyman-break feature. The host galaxy is a small starburst galaxy with moderate intrinsic extinction ($A_V = 0.3$) and has a SFR of $\sim 60 M_{\odot}/$ yr typical for LBGs. It is one of the few cases where a GRB host has been found to be a classical Lyman-break galaxy. Using the redshift we estimate the isotropic-equivalent radiated energy of the burst to be $E_{iso} = (1.15 \pm 0.20) \times 10^{54}$ erg. We also provide evidence in favour of the hypothesis that the darkness of GRB 051008 is due to local absorption resulting from a dense circumburst medium.

**Key words:** gamma-ray bursts: host galaxies

## 1 INTRODUCTION

Cosmic gamma-ray bursts (GRBs) are among the most powerful events in the Universe. A detection of a GRB is expected to be followed by the detection of an afterglow in other spectral ranges: X-ray, optical, and radio emissions. Presently, a large number of ground-based robotic telescopes search for optical afterglows rapidly after GRBs have occurred. Also, on-board the dedicated *Swift* space observatory (Gehrels et al. 2004), the UltraViolet/Optical Telescope (UVOT, Roming et al. 2005) is used for rapid follow-up of UV and optical afterglows. However, it is now clear that for a substantial fraction of events (from 20%, Cenko et al. 2009; Greiner et al. 2011, to 35%, Melandri et al. 2012) we are currently unable to detect any optical afterglow, even with rapid follow-up within the first minutes after the GRB (see also Fynbo et al. 2001; Lazatti, Covino & Ghisellini 2002).

Faintness or the complete lack of an optical afterglow (OA)

⋆ email: alinusss@gmail.com
† email: apozanen@iki.rssi.ru

may be caused by different factors. Most prosaically, a failure to detect the OA may be due to the low limiting magnitude of the observations, such as when only small robotic telescopes observe the GRB position early on (in contrast to larger rapid follow-up telescopes, see Greiner et al. 2011).

A possible factor for a GRB to be dark is the immediate neighbourhood of its source. The "extinction scenario" (Taylor et al. 1998) assumes that the emission of the OA is strongly absorbed in the host galaxy. Moreover, the GRB source may be surrounded by a dense circumburst medium (Paczynski 1998; Galama & Wijers 2001).

Another potential origin of dark bursts is a high redshift. Emission with wavelengths shorter than $912(1+z)$ Å in the observer frame is efficiently absorbed due to the Lyman-cutoff when it passes through the intergalactic medium (Lamb & Reichart 2000)[1]. For $z \geqslant 4$, this Lyman drop-out falls into the $R_C$ band in the optical in which most rapid searches for GRB afterglows are carried out. Such GRBs can only be localized through rapid, deep near-infrared (NIR) follow-up, e.g., as in the case of GRB 080913 (Greiner et al. 2009; Pérez-Ramírez et al. 2010).

To determine whether the burst is genuinely dark, due to some physical factors rather than to an inefficient search, it is useful to compare the observed optical/near-IR detections or upper limits with the values expected from the brightness of the X-ray afterglow. This approach is based on the standard fireball model (Sari, Piran & Narayan 1998), where the afterglow spectrum produced by the synchrotron radiation follows the simple power law $F_\nu \sim \nu^{-\beta}$. Jakobsson et al. (2004) proposed to define dark bursts using an optical to X-ray spectral index $\beta_{OX} < 0.5$, since in log space it is the shallowest expected slope of the synchrotron spectrum in the standard afterglow model. Alternatively, van der Horst et al. (2009) uses the value of the X-ray spectral index $\beta_X$, assuming for the definition of dark bursts the condition $\beta_{OX} - \beta_X < 0.5$.

Finally, the burst may be intrinsically faint and the low optical luminosity of its OA may be due to a low density of the interstellar medium into which the relativistic outburst of the GRB propagates (Sari, Piran & Narayan 1998, note that in this case a GRB may not be dark according to the Jakobsson criterion, as it may also have a very faint X-ray afterglow).

Long GRBs are known to be linked to the deaths of massive stars, and hence to star-formation activity (Jimenez & Piran 2013). As a result, one may expect some GRBs to be located in dusty environments, with high extinction values along the lines of sight towards the bursts, or even high bulk extinction in the host galaxies. Melandri et al. (2008) found that about 50% of *Swift* dark bursts show evidence of a mild extinction. Further studies by Perley et al. (2009) showed that the majority of dark bursts require $A_V^{host} \geqslant 1$ mag, with a few cases reaching $\sim 2-6$ mag. There are many notable examples of highly extinguished events: GRB 980828 (Djorgovski et al. 2001); GRB 051022 (Castro-Tirado et al. 2007); GRB 061222A (Perley et al. 2009); GRB 070306 (Jaunsen et al. 2008); GRB 070521 (Perley et al. 2009); GRB 080325 (Hashimoto et al. 2010); GRB 080607 (Chen et al. 2010; Perley et al. 2011); GRB 090417B (Holland et al. 2010); GRB 100621A (Greiner et al. 2013); GRB 110709B and GRB 111215A (Zauderer et al. 2013).

The study of properties of host galaxies is one of the tools for investigating the environment in which the GRBs form (e.g., Savaglio et al. 2009). Recent research on large populations of dark-GRB host galaxies has shown that generally, they do not differ from the host galaxies of GRBs that suffer from little dust extinction (Perley et al. 2009), with the "darkness" being mostly due to local extinction around the progenitor in galaxies of low to medium redshifts. But one can note that some very dark GRBs trace a population of extremely red host galaxies (Hunt et al. 2011; Rossi et al. 2012; Svensson et al. 2012), whereas highly extinguished (but still detected) GRB afterglows are preferentially linked with more massive host galaxies (Krühler et al. 2011). The host galaxies of dark GRBs in general have large SFRs (Perley et al. 2013).

Redshifts of detected host galaxies vary in a wide range from $z = 0.0085$ (GRB 980425 Tinney et al. 1998) to $z = 4.667$ (GRB 100219A Thöne et al. 2013) with a median value of $z_{host}$ about 1.4[2]. About 20% of discovered GRB host galaxies lie at redshifts more than 2.5. The search for and spectroscopic observations of galaxies with $z \geqslant 2.5$ is a non-trivial problem. In these cases techniques of photometric redshift estimation are useful. E.g., the Lyman limit of hydrogen at 912 Å in the rest frame of a galaxy helps to find ordinary starburst galaxies at $z \sim 3$ and at higher redshifts to identify Lyman break galaxies (LBGs). But to date there were only a few associations between GRBs and LBGs (Odewahn et al. 1998; Malesani et al. 2013). Also if GRBs trace star-formation one should expect that a typical GRB host galaxy at $z > 2.5$ will be under-luminous and fall below $L^*$ of the LBG luminosity function (Jakobsson et al. 2005a; Fynbo et al. 2008). In the case of dark bursts the discovery of the host galaxy is often the only way to determine the distances to these sources and to try to obtain an insight into their nature (e.g., Jakobsson et al. 2012; Krühler et al. 2012a).

In this paper we determine and discuss properties of GRB 051008 and its host galaxy. We present detailed parameters of the prompt $\gamma$-ray emission observed by Konus-*WIND* in the energy range up to 14 MeV which is essential for determining the physical parameters $E_p$ and $E_{iso}$. We also report new observations of the host galaxy which were not published earlier in preliminary studies (Volnova et al. 2010a,b). In particular these observations in $U$, $g'$, $R$, $I$, and $Z$ bands provided by the Keck I telescope, in $K'$ band provided by the Gemini North telescope, and ultra-violet observations provided by *Swift*/UVOT helped us to determine a secure photometric redshift of the galaxy. In the paper we use the following notations and conventions: time-decay, photon, and spectral indices are indicated with $\alpha$, $\Gamma$, and $\beta$, following the standard convention $t^{-\alpha}$, $N_{ph}^{-\Gamma}$, and $\nu^{-\beta}$, respectively. We use the following cosmological parameters $H_0 = 71$ km/s/Mpc, $\Omega_M = 0.27$, $\Omega_\Lambda = 0.73$ and cosmological calculations of Ned Wright's Cosmology Calculator (Wright 2006). If not stated otherwise, all errors represent one standard deviation, and upper limits are three standard deviations for the parameter of interest.

## 2 THE GAMMA-RAY BURST GRB 051008

### 2.1 Detection of the burst

The gamma-ray burst GRB 051008 was detected by the BAT telescope of the *Swift* space observatory at 16:33:21 UT on October 8, 2005 (Marshall et al. 2005). The burst occurred during a telemetry downlink transmission and that is why the corresponding alert was not received by the BACODINE $\gamma$-ray alert network [3] until 10 minutes after the event. The spacecraft did not slew to the burst

[1] At higher redshifts the Ly$\alpha$ forest becomes effectively opaque causing the break to be at $1217(1+z)$ Å

[2] http://www.grbhosts.org/

[3] S. Barthelmy, `http://gcn.gsfc.nasa.gov/`

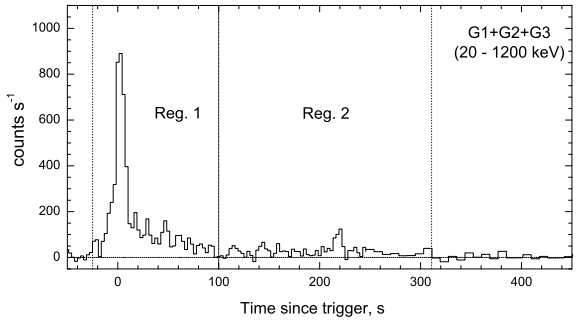


**Figure 1.** An overview of the Konus-*WIND* light curve. The background-subtracted time history in the G1+G2+G3 bands is presented. The fluence calculation intervals are tagged as *Reg. 1* and *Reg. 2*.

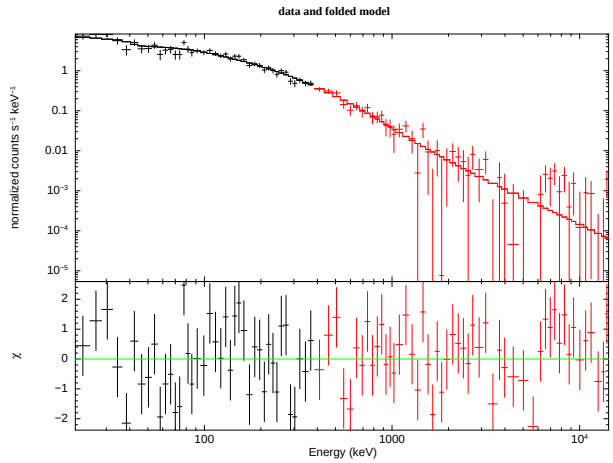


**Figure 2.** The Konus-*WIND* energy spectrum measured from $T_0$ to $T_0$+8.2 s and its fit with the Band function (see Table 3 for details).

immediately because of the Earth-limb observing constraint. This condition also prevented *Swift*/BAT from recording all gamma radiation from the event (see Section 2.2). This burst was also detected at 16:33:18 UT by the WAM $\gamma$-ray monitor on-board the *Suzaku* observatory and had a duration of 48 s in the energy range from 100 keV to 2 Mev. The burst spectrum in this energy range can be fitted fairly well by a CPL model with $dN/dE \sim E^{\Gamma}e^{-E/E_c}$ with photon index $\Gamma = -1.24 \pm 0.15$, and a cut-off energy of $E_c = 1535^{+1419}_{-561}$ keV (Ohno et al. 2005).

GRB 051008 was also recorded by Konus-*WIND* (see Section 2.2), as well as the SPI-ACS detector on-board *INTEGRAL* observatory (see Section 2.3), and the Mars Observer spacecraft [4].

### 2.2 Konus-*WIND* observations

GRB 051008 triggered detector S2 of the Konus-*WIND* $\gamma$-ray spectrometer (Aptekar et al. 1995) at $T_0$=16:33:21 UT. As derived from the *WIND* spacecraft ephemerides and the *Swift* localization of the GRB source, the corresponding Earth-crossing time is $T_\oplus$ = $T_0$+2.8 s.

[4] http://www.ssl.berkeley.edu/ipn3/masterli.txt

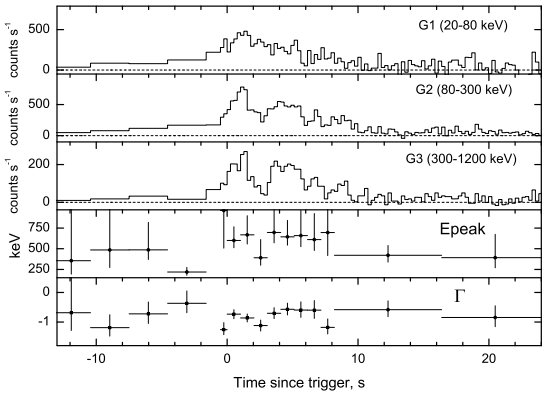


**Figure 3.** Spectral evolution of the prompt $\gamma$-ray emission during the main phase of the burst. Background-subtracted light curves in three energy bands (G1, G2, G3) are shown, along with the temporal behaviour of the CPL spectral model parameters $E_{peak}$ and $\Gamma$.

**Table 1.** GRB 051008 energy fluence measured with Konus-*WIND*.

| Time interval (s) | Spectral range, keV | Fluence, $10^{-5}$ erg cm$^{-2}$ |
|---|---|---|
| Region 1[a] ($T_0$-25 to $T_0$+98) | 20 – 14000 | $5.9 \pm 1.0$ |
| Region 2 ($T_0$+98 to $T_0$+311) | 20 – 14000 | $0.8 \pm 0.5$ |
| Whole burst ($T_0$-25 to $T_0$+311) | 20 – 14000 | $6.7 \pm 1.1$ |

[a] The fluence for the pre-trigger part (from $T_0$-25 s to $T_0$) is estimated using a product of the count fluence for this part and the conversion factor from a count fluence to an energy fluence using the spectral information of the time-averaged spectrum.
[b] All the quoted errors are at the 90% confidence level.

In the triggered mode, the burst time histories are recorded by the instrument in three energy bands: G1 (20–80 keV), G2 (80–300 keV), and G3 (300–1200 keV). The measurement started from 0.5 s before and up to 229.6 s after the spacecraft trigger, with a time resolution varying from 2 ms up to 256 ms. The time history of the burst is also available from the instrument's waiting-mode data, which are recorded up to $T_0$+250 s in the same energy bands

**Table 2.** Spectral lag between Konus-*WIND* light curves in the time interval [0 – 10 s]

| Light curves | Time scale (ms) | $\tau^a_{lag}$ (s) |
|---|---|---|
| G3 – G1 | 256 | $-0.2 \pm 0.3^b$ |
| G2 – G1 | 256 | $-0.16 \pm 0.14$ |
| G3 – G2 | 64 | $0.06 \pm 0.06$ |

[a] In this table positive spectral lag means that the spectrum has hard-to-soft evolution. [b] All the quoted errors are at 1 $\sigma$ level.

**Table 3.** Summary of Konus-*WIND* spectral fits in 0.02–14 MeV energy range.

| Time interval (s) | Spectral model | $\Gamma$ | $E_{peak}$ (keV) | $\Gamma_2$ | $\chi^2$/dof |
|---|---|---|---|---|---|
| Central part | Band | -0.95 (-0.10,+0.12)[a] | 660 (-161,+183) | -2.34 (-1.23,+0.24) | 101/88 |
| ($T_0$ to $T_0$+8.2) | CPL | -1.00 (-0.08,+0.09) | 770 (-123,+162) | – | 105/89 |
| | PL | -1.46 (-0.02,+0.02) | – | – | 306/90 |
| Main pulse | Band | -0.75 (-0.28,+0.40) | 307 (-101,+195) | -2.10 (-0.59,+0.20) | 97/96 |
| ($T_0$ to $T_0$+98) | CPL | -1.06 (-0.15,+0.18) | 563 (-157,+291) | – | 101/97 |
| | PL | -1.51 (-0.04,+0.04) | – | – | 185/99 |
| Tail | PL[b] | -1.97 (-0.32,+0.39) | – | – | 117/98 |
| ($T_0$+98 to $T_0$+311) | | | | | |

[a] All the quoted errors are at the 90% confidence level.
[b] In this region parameters of the CPL and Band models are not constrained.

with 2.944 s time resolution. A search for a possible precursor to the burst was performed using this data set, with no statistically significant positive result up to $T_0$-1500 s.

As observed by Konus-*WIND*, the burst light curve shows a multi-peaked hard-spectrum pulse which starts at $\sim$ $T_0$-25 s and decays to $\sim$ $T_0$+100 s (Fig. 1). Additional information about the burst light curve after $T_0$+250 s can be extracted from the multichannel spectra which are measured up to $T_0$+490 s. The analysis of these data shows that the $\gamma$-ray emission continues, mostly in the soft G1 band, up to $\sim$ $T_0$+310 s. The total burst duration $T_{100}$=246.1 s was determined at the 5$\sigma$ level in the 20–1200 keV band. The corresponding value of $T_{90}$ is 214$\pm$30 s and $T_{50}$ =48$\pm$4 s.

During the burst the instrument measured 64 multichannel energy spectra covering two partially overlapping energy ranges: PHA1 (20–1200 keV) and PHA2 (0.4–14 MeV). The spectral analysis was performed using XSPEC V12.5 (Arnaud 1996) by applying three spectral models. The first one is a simple power-law (PL): $f(E) \propto E^{\Gamma}$ where $\Gamma$ is the power-law photon index. The second model is a power-law with an exponential cut-off, parametrized as $E_{peak}$: $f(E) \propto E^{\Gamma} exp(-(2+\Gamma)E/E_{peak})$ where $E_{peak}$ is the peak energy in the $\nu$F$_\nu$ spectrum. The third model is the Band function (Band et al. 1993): $f(E) \propto E^{\Gamma} exp(-(2+\Gamma)E/E_{peak})$ for $E < E_{peak}(\Gamma-\Gamma_2)/(2+\Gamma)$, and $f(E) \propto E^{\Gamma_2}$ for $E \geqslant E_{peak}(\Gamma-\Gamma_2)/(2+\Gamma)$ where $\Gamma_2$ is the photon index in the higher energy band.

A summary of the Konus-*WIND* spectral fits is presented in Table 3. The spectrum of the brightest part of the burst (measured from $T_0$ to $T_0$+8.192 s) is best fitted in the 20–14000 keV energy range with the Band model ($\chi^2$=101/88 dof) (see Fig. 2). The CPL function yields a fit result of similar quality ($\chi^2$=105/89 dof). For both mentioned models relatively high values of $E_{peak}$ $\sim$700 keV are obtained, placing this burst among the hardest of the Konus-*WIND* long GRBs. The time-integrated spectrum of the main part of the GRB (measured from $T_0$ to $T_0$+98.3 s) is also best fitted by the Band function with $E_{peak} = 307^{+195}_{-101}$ keV ($\chi^2$=97/96 dof). Considering a spectrum of the final part of the burst (from $T_0$+98.3 to $T_0$+311.3 s) the only model for which the fit parameters are constrained is a simple power-law function yielding the photon index $\Gamma$ close to -2 ($\chi^2$=117/98 dof).

Based on the results of the spectral analysis the observed burst energetics parameters such as energy fluence (Table 1) and peak energy flux are calculated. The latter value reaches $F_{max} = (7.0 \pm 0.7) \times 10^{-6}$ erg cm$^{-2}$ s$^{-1}$ in a 64 ms time interval starting at $T_0$+1.1 s. The total energy fluence of the burst amounts to $S = (6.5 \pm 1.1) \times 10^{-5}$ erg cm$^{-2}$. Both values are measured in the 20 keV – 10 MeV energy range, standard for calculations of the Konus-*WIND* GRB energetics, and the quoted errors are at the 90% confidence level.

It is possible to consider the GRB time history in the three energy bands (G1, G2, G3) as a series of three-channel energy spectra. In this case the spectral variability of the burst can be studied on a faster time scale (Mazets et al. 2001; Ulanov et al. 2005). We applied this method to the GRB 051008 light curve in order to obtain the fine temporal behaviour of the CPL spectral model parameters $E_{peak}$ and $\Gamma$ during the brightest phase of the burst. As a result (Fig. 3) clear evidence of spectral variability in the form of a hardness-intensity correlation is obtained (particularly between $E_{peak}$ and the light curves above 80 keV).

We also examined the spectral lag $\tau_{lag}$ using the cross-correlation function (CCF) between the light curves in two energy bands (Norris, Marani & Bonnell 2000; Band 1997). After calculating the CCF as a function of the lag $\tau_{lag}$ we obtained the peak value of $\tau_{lag}$ by fitting it with a fourth-degree polynomial. The resulting values of $\tau_{lag}$ between the G1, G2, and G3 light curves in different combinations are listed in Table 2. As one can see none of these values differ from zero by more than one standard deviation and thus a negligible spectral lag is evident (see also Section 2.3). This result places GRB 051008 among the 17% of zero-lag events of the Konus-*WIND* sample of $\sim$ 950 long GRBs with well-determined spectral lags[5].

### 2.3 *INTEGRAL* observations

The burst was detected by the SPI-ACS detector on-board the *INTEGRAL* observatory at 16:33:12 UT[6]. The burst position was $\theta$ = 86 degrees off the axis of the aperture telescopes. The SPI-ACS continuously records count rates in a single wide energy band $\sim$ (80–10000) keV with a time resolution of 50 ms (von Kienlin et al. 2003). Owing to the large size of the SPI-ACS detector (geometrical surface area is 5250 $cm^2$ at the $\theta = 90$) significant ($3\sigma$) emission was detected up to 800 s after the burst trigger (Fig.4). We again searched for a possible precursor but did not find one in the

[5] Svinkin et al., 2014, in preparation
[6] http://www.isdc.unige.ch/*INTEGRAL*/ibas/cgi-bin/ibas_acs_web.cgi/?trigger=2005-10-08T16-33-12.1588-07660-00007-0

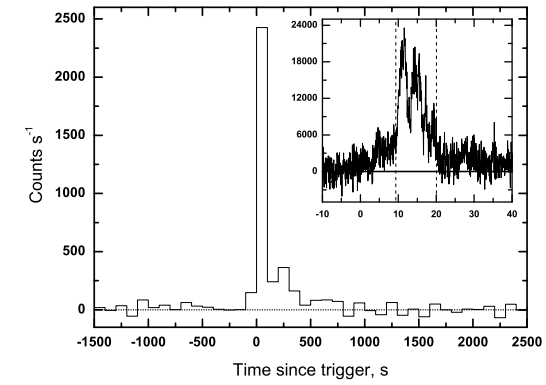


a)

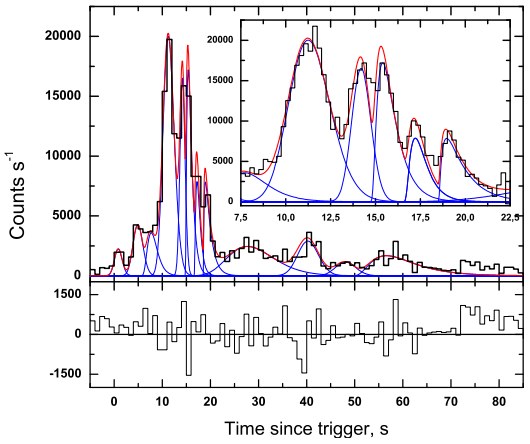


b)

**Figure 4. a)** Background-subtracted light curve of GRB 051008 obtained by the *INTEGRAL*/SPI-ACS in the energy band $\sim$ 80 keV – 10 MeV. Here, the original light curve with a time resolution of 50 ms has been re-binned into 100 s bins. Inset: the light curve of the main peak of the burst; the dashed lines denote the time interval for the PDS calculation, see Section 2.3. **b), top panel** The light curve at 1 s time resolution fit with a number of single pulses; **b), bottom panel** Residuals.

range of $T_0 - 1500$ s. The $T_{90}$ in the energy band of SPI-ACS is $535 \pm 40$ s.

Using the original time resolution we searched for a possible periodicity of the whole light curve. No significant periodicity was found on time scales from 0.1 to 20 s. We also investigated the power spectrum of the main peak of the burst in the time interval [10–20] s after trigger (see inset in Fig.4). The power density spectrum (PDS) can be fitted by a single power-law with index of $-2.06 \pm 0.09$ up to 7 Hz. The power-law index significantly differs from the index $\sim$ 1.6 of averaged PDS obtained for long GRBs (Beloborodov et al. 2000; Pozanenko & Loznikov 2000).

GRB 051008 is a good example of a multi-peak event. Using SPI-ACS data and technique developed early (Minaev et al. 2014) we found at least 10 separated pulses which fit the light curve fairly well (Fig.4b). We cannot investigate the spectral lag of the separate pulses due to heavy overlap of the pulses. It was found the existence of the lag vs. pulse duration correlation (Hakkila et al. 2007; Minaev et al. 2013, 2014), i.e. the shorter pulse, the smaller spectral lag corresponds to the pulse. It is multi-peak structure of short duration pulses composing the main body of a burst light curve could

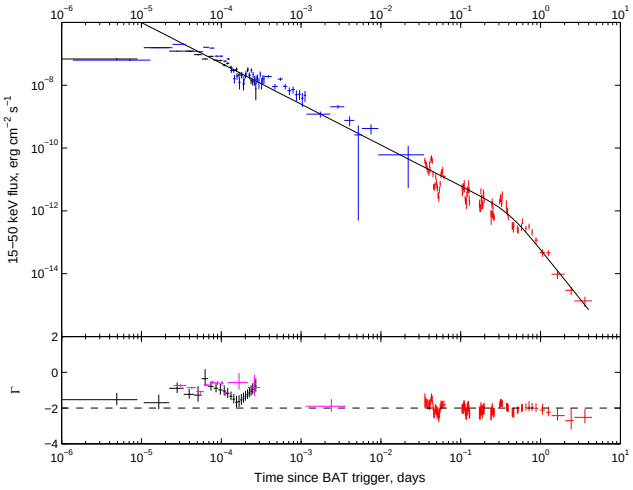


**Figure 5. (top)** The 15–50 keV X-ray light curve of GRB 051008 based on the data from the *Swift*/BAT (black crosses), *Swift*/XRT (red crosses), and *INTEGRAL*/SPI–ACS (blue crosses). The black solid line represents the best fit to the data using a broken power-law (1); **(bottom)** photon indices Γ of the X-ray spectrum obtained by *Swift*/BAT (black crosses), *Swift*/XRT (red crosses), and Konus-*WIND* (magenta crosses).

be the underlying nature of a negligible lag of the GRB 051008 as a whole (see Table 2, Fig. 4).

Since the lag of the whole burst is not an additive function of the lag of separate pulses even superposition of pulses with positive lags may result in a negative lag of a complex of superimposed pulses (Minaev et al. 2014). This is another plausible reason of the negligible lag of the GRB 051008.

### 2.4 *Swift*/XRT observations

The XRT X-ray telescope (Burrows et al. 2005) on-board the *Swift* space observatory began observing the region of the burst at 17:23:52 UT, i.e., 50 minutes after the BAT trigger. The XRT detected the fading X-ray source (Perri, Capalbi & Burrows 2005a) which was identified as the X-ray afterglow of the burst. Butler (2007) provided an on-ground SDSS-enhanced position of the X-ray afterglow at RA $= 13^h31^m29\overset{s}{.}55$, Dec. $= +42°05'53\overset{''}{.}3$ with an accuracy of $1\overset{''}{.}2$ (90% confidence level). For additional information on the X-ray afterglow analysis see Margutti et al. (2013).

Fig. 5 shows the flux light curve in the 15–50 keV energy range created using BAT, XRT[7], and SPI-ACS data. The flux light curve can be created from a count-rate light curve using a conversion factor computed from spectral and absorption models and instrumental response matrices. The procedure is not unreasonable if the photon index (Γ) varies smoothly with time (for more details see Evans et al. 2010). Indeed the photon index (Fig. 5, bottom panel) is seen to be monotonously decreasing from the end of the BAT data toward XRT via the Konus-*WIND* data in between.

Since the SPI-ACS experiment has no spectral channels we converted the SPI-ACS count-rate light curve into a flux light curve in the energy range 15–50 keV in two steps. (1) Using the Konus-*WIND* CPL spectral model we calculated the fluence of the main activity episode (-25 s – 98 s) in the 80 keV - 10 MeV energy range

[7] http://www.swift.ac.uk/burst_analyser/00158855/SHOWbat_xrt_lightcurves/TIMEDEL1/bat_xrt_flux_with_gamma_BATBAND_BATTIMEDEL1.qdp.gz

(i.e., the SPI-ACS energy band), and we found a conversion coefficient (at the same time interval of the SPI-ACS) which is equal to $(2.5 \pm 0.7) \times 10^{-10}$ erg/cm$^2$ per count. (2) Using the same CPL spectral model we converted the SPI-ACS fluence into the 15–50 keV energy range.

The resulting BAT+SPI-ACS+XRT flux light curve was fitted by a broken power-law (see, e.g., Beuermann et al. 1999):

$$F = F_0 \left[ \left( \frac{t}{t_b} \right)^{\alpha_1 w} + \left( \frac{t}{t_b} \right)^{\alpha_2 w} \right]^{-1/w}, \quad (1)$$

where $\alpha_1$ and $\alpha_2$ are the initial and final flux decay indices; $t_b$ is the time corresponding to the break in the light curve; $w$ is the parameter responsible for the sharpness of the break, and $F_0$ is the normalization coefficient. Figure 5 shows the light curve with the fit. The fit yields the following parameter values: $t_b = 0.41 \pm 0.14$ days, $\alpha_1 = 1.30 \pm 0.18$, and $\alpha_2 = 3.18 \pm 0.20$. Among tested discrete values of break sharpness from 1 to 5 the best-fitted $w$ equals 2.

The $t_b = 0.41 \pm 0.14$ days is somewhat larger than the one obtained in Racusin et al. (2009) ($t_b = 0.19 \pm 0.04$ days). It could be due to different light-curve models being used, but primarily due to adding *Swift*/BAT and *INTERGRAL*/SPI-ACS data to the fit. Indeed, if we fit only the *Swift*/XRT data (Volnova et al. 2010a), we find this parameter to be in a good agreement with the results of Racusin et al. (2009). It is also evident that the afterglow light curve of GRB 051008 belongs to a less frequent class of plateauless XRT light curves and may represent only phases III and IV of the canonical X-ray afterglow (Racusin et al. 2009; Zhang et al. 2006; Nousek et al. 2006; Liang et al. 2009).

### 2.5 Optical and NIR observations

The Crimean Astrophysical Observatory started observations of the burst error box with the 2.6-m Shajn telescope 32 minutes after the burst trigger (Rumyantsev, Biryukov & Pozanenko 2005). Close to the initial XRT error circle a source (Id1 in Fig. 6) was found, which however was later discarded as the OA of GRB 051008 (Pozanenko et al. 2007). The limiting $R$ magnitude of the co-added frame with mean observing time 17:28:14 UT is $23\overset{\mathrm{m}}{.}3$.

The UVOT optical telescope of the *Swift* space observatory started to monitor the region of GRB 051008 at 17:23:49 UT, 50 minutes after the burst trigger (Roming, Marshall & Blustin 2005). The telescope took a 200-s $v$-band image, no afterglow was found at a 5-$\sigma$ significance level for $18\overset{\mathrm{m}}{.}2$ (Breeveld et al. 2005). The optical observations of the burst region were highly hindered by the presence of the bright $R \sim 5\overset{\mathrm{m}}{.}5$ star HR 5096 $2'.5$ from the XRT position.

*Swift*/UVOT continued observations of the GRB 051008 region up to Oct.14 using the ultraviolet filters $u, uvw1, uvm2$ and $uvw2$, with a total exposure of about 11000 seconds in each filter, and the $v$ filter with a total exposure of more than 120000 s. Neither OT nor the host galaxy of the GRB was detected in stacked images in any UVOT filter, particularly up to $uvw2 > 23.2$.

Observations of the field of GRB 051008 were obtained with the 1.34m Schmidt telescope of the Thüringer Landessternwarte Tautenburg as soon as dusk fell, beginning 0.8 hours after the GRB trigger (see Klose & Hoegner 2005; Ferrero & Klose 2005; Ferrero et al. 2005). Initial observations were obtained in the $I_C$ band, lengthening the exposure times ($2 \times 10$ s, $6 \times 20$ s, $7 \times 120$ s) in order to accommodate for the decrease in sky background. These observations were followed by sets of $6 \times 120$ s each in $R_C$ and $V$. The halo of the bright nearby star influences the GRB position only in the $R_C$ image, reducing the limiting magnitude.

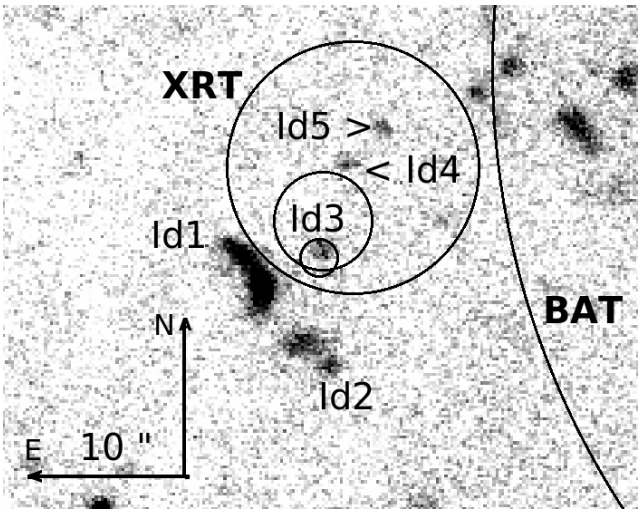


**Figure 6.** The localization of GRB 051008 and its immediate neighbourhood. The image was taken 255 days after the GRB in the $R$-band filter (the limiting magnitude is $25\overset{\mathrm{m}}{.}7$) with a 4800 s exposure, using the NOT. The burst error circles determined from the *Swift*/BAT and the *Swift*/XRT telescopes data are shown with solid lines. An arc at the right side of the image is a part of BAT error circle. Three small circles denote different XRT error boxes. The position of the X-ray afterglow of the burst lies outside the refined BAT error circle. The smallest error box depicts the *Swift*/XRT refined error circle at (J2000) RA $= 13^h31^m29\overset{\mathrm{s}}{.}55$, Dec. $= +42^\circ05'53''.3$ with a radius of $1''.2$ (Butler 2007). The Id1–5 markers indicate the sources studied in this paper. The coordinates of the Id3 source are RA $= 13^h31^m29\overset{\mathrm{s}}{.}510$, Dec. $= +42^\circ05'53''.67$ (J2000) with an error of $0''.08$ in both right ascension and declination (statistical error only). The image scale and seeing are equal to $0''.19$ per pixel and $0''.9$, respectively.

We obtained further imaging with the TLS Schmidt $\sim 20$ days after the GRB, around the expected peak-time of a low-$z$ GRB supernova (Zeh, Klose & Hartmann 2004; Ferrero et al. 2005). We obtained $30 \times 60$ s exposures in the $I_C$ band, and then $3 \times 30 \times 60$ s exposures in the $R_C$ band in three consecutive nights. These observations were all obtained at high airmass (1.8 – 3.0). For the 90 minute stacked $R_C$ image, we carefully modelled and subtracted the flux of the nearby bright star. While strong residuals remain within $20''$ of the star's position, the GRB location is far enough away to have a smooth background. We clearly detect the galaxy Id1 and faintly detect the galaxy Id2 next to it. At the XRT position of the X-ray afterglow (and the host galaxy Id3 underneath it), no source is detected to $R_C > 22.7$. The $I_C$ upper limit is significantly less deep and not constraining.

All TLS data were calibrated against two bright but non-saturated SDSS DR8 stars (stars 6 and 7 in Table 6), as the other stars were in most cases not even detected. SDSS AB magnitudes were transformed into Johnsons-Cousins Vega magnitudes analogue to the other calibration stars.

On April 28, 2006 a source candidate for the host galaxy of GRB 051008 was found as a result of observations made with the Shajn telescope of the Crimean Astrophysical Observatory (see Fig.6, source Id3). The source was further observed in 2006–2009 with the Nordic Optical Telescope (NOT), the AZT-22 telescope of the Maidanak Observatory, and the Keck telescope. These observations allowed us to take images of the burst region in the $Bg'VRR_CI_C$ filters and in the interference filter $i$. In February 2008 and in February–March 2012 we obtained additional optical observations of the field using the Low Resolution Imaging Spec-

trometer (LRIS) on Keck. The series of frames were taken in the $UBIZ$ filters with total exposure times of 930, 930, 810, and 720 seconds, respectively. All preliminary reductions were performed using private IDL codes. The best limiting magnitude was obtained in the filter $g' > 27\overset{\rm m}{.}2$, for the other limiting magnitudes see Table 4.

We acquired deep infrared imaging at the position of GRB 051008 using the Near-Infrared Imager (NIRI) on Gemini-North on the night of 2010 June 23, starting at 07:15 UT. 27 exposures of 60 seconds each were acquired on the field in the $K'$ filter, which we reduced and stacked using the routines in the Gemini IRAF package. Unfortunately, there is only a single faint star (2MASS 13313142+4206470) in the FOV of the combined image, which a series of late-time PAIRITEL images suggests may be variable. Instead, since the night was photometric, we calibrate the host photometry using an observation of the IR standard star FS 29 taken later in the night of Gemini observations.

Table 4 presents the log of our observations of the GRB 051008 field. Fig. 6 displays the location of GRB 051008, indicating the supposed host galaxy, and the XRT and BAT error circles. Galaxies Id1, Id2, Id4, and Id5 lie within a 10 arcsecond radius circle around the probable host galaxy of GRB 051008 (Id3) and we will also study these galaxies below. Table 5 gives the results of the photometric reduction of the observations of this region.

All astrometric solutions were obtained using the APEX astrometric code (Devyatkin et al. 2010). All astrometric errors are statistical only if not stated otherwise. The reference catalogue for the astrometric reduction is USNO-B1.0. All photometric calibrations for the data employed in this paper were performed using the method of relative aperture photometry via the APPHOT procedure of the IRAF software package[8] except for the *Swift*/UVOT data which were reduced using NASA's HEASARC software package HEAsoft[9]. The Id1 and Id2 sources have complex shapes and using the APPHOT procedure we therefore applied the apertures shaped as irregular closed polygons inscribed in the isophotes. For the photometric calibration of the $Bg'VRI$ images we used seven stars from the SDSS-DR7 catalogue (Abazajian et al. 2009) (see Table 6)[10]. The transmission curves of the Keck $U$ and $Z$ filters do not match exactly the SDSS $u$ and $z$ bands. The $U$ and $Z$ images were calibrated using the relative magnitude averaged by 14 non-overexposed stars of the field. The stars were chosen with the aid of an on-line software package which we use to search for secondary photometric standards in the FOV of GRBs from automatic GCN notices (BACODINEs).[11] To process *Swift*/UVOT data we used the task UVOTIMSUM of the HEAsoft package to combine all frames for each filter ($u, uvw1, uvm2, uvw2$ and $v$) and the task UVOTSOURCE to obtain the magnitudes of the sources Id1–5. The calibration and upper limit estimates were done using the HEASARC CALibration Data Base (CALDB[12]). For the galaxies Id3–5 we used circular apertures with a fixed radius of $2\overset{''}{.}2$. For the Id1 and Id2 galaxies we increased this radius to $5\overset{''}{.}0$.

[8] http://iraf.noao.edu/

[9] http://heasarc.nasa.gov/docs/software/lheasoft/

[10] Magnitudes are converted from the *ugriz* into the *BVRI* system using Lupton's transformations http://www.sdss.org/dr7/algorithms/sdssUBVRITransform.html

[11] Pozanenko et al., in preparation.

[12] http://heasarc.gsfc.nasa.gov/FTP/caldb

### 2.6 Spectroscopy of the host galaxy

We obtained a longslit spectrum of the host galaxy of GRB 051008 on the night of 2009 June 25 (UT) using the Low-Resolution Imaging Spectrometer (LRIS, Oke et al. 1995) on the Keck I 10-meter telescope. Three exposures of 900 seconds each were acquired on the source at a position angle of 202 degrees, using the D560 dichroic, 600-line grism (blue), and 400-line grating (red). The target was acquired independently before each of the three 900 s exposures and no additional dithering was performed, so the exposures are effectively undithered aside from small differences of less than 1 arcsecond. No obvious line features are identified in the sky-subtracted 2D spectra.

### 2.7 Radio observations

GRB 051008 was observed by the Very Large Array. No radio afterglow was detected. An 8.5 GHz flux upper limit of 0.12 mJy was obtained for the burst location region on Oct. 8, 2005, at 20:30:24 UT, i.e., four hours after the trigger (Cameron 2005, see also Chandra & Frail 2012). Further observations carried out 2 days after the trigger on Oct. 10, 18:57:36 UT at the same frequency obtained a flux upper limit of 0.11 mJy[13].

The position was also re-observed on June, 11, 2012 with the upgraded Karl G. Jansky Very Large Array as part of the host-galaxy study of Perley & Perley (2013). No source was detected consistent with the XRT position with a $2\sigma$ upper limit of 0.014 mJy at 5.23 GHz.

## 3 PROPERTIES OF THE HOST GALAXY

The coordinates of the Id3 source (Fig. 6) are RA $= 13^h31^m29\overset{s}{.}510$, Dec. $= +42°05'53\overset{''}{.}67$ (J2000), accurate to within $0\overset{''}{.}08$ in both coordinates (statistical error). The source lies inside the final XRT $1\overset{''}{.}2$-error box corrected using the joint observations of the source field performed by the XRT and the centroids of corresponding optical sources in the SDSS-DR5 catalogue (Butler 2007). However, this match may be accidental. Bloom et al. (2002) reported a formula for computing the probability of finding a galaxy inside an arbitrary sky area as a function of the galaxy magnitude. For GRB 051008 it yields a probability of about $1.96\%$ for an accidental location of the Id3 galaxy inside the XRT error circle.

In a circle with centre at Id3 and radius of $10''$ there are 5 galaxies. One can assume that these galaxies compose a group. We will investigate it below.

We used the *Le Phare* software package (Arnouts et al. 1999; Ilbert et al. 2006) to estimate the redshifts of the galaxies Id1–5 from the photometric data obtained with the NOT, Keck I, and Gemini North. We found a photometric redshift of $z = 2.77^{+0.15}_{-0.20}$ (95% confidence level) for the host galaxy. An independent analysis of the redshift based only on the Keck observations shows $z = 2.90^{+0.29}_{-0.16}$ at the same confidence level (Perley et al. 2013). Table 7 lists the estimated redshift values and other parameters of the galaxies Id1–5 including those determined using *Le Phare*: the most probable galaxy SED type, the best-fitted extinction law, internal bulk extinction in the galaxy, and age of the dominant stellar population of the galaxy. We used the PEGASE2 population synthesis models library (Fiok & Rocca-Volmerange 1997) to obtain

[13] http://www.aoc.nrao.edu/∼dfrail/grb051008.dat

**Table 4.** Log of optical and NIR observations of the GRB 051008 location. The magnitudes are not corrected for Galactic reddening.

| Date | $t - t_0$, days | Telescope | Exposure, s | FWHM, $''$ | Filter | Upper limit, at the $3\sigma$ level |
|---|---|---|---|---|---|---|
| 8.10.2005 | 0.034 | TLS | 20 | 1.3 | $I_C$ | 16.0 |
| 8.10.2005 | 0.035 | ZTSh | 2200 | 2.1 | $R_C$ | 23.3 |
| 8.10.2005 | 0.041 | TLS | 120 | 1.3 | $I_C$ | 17.5 |
| 8.10.2005 | 0.049 | TLS | 840 | 1.4 | $I_C$ | 19.3 |
| 8.10.2005 | 0.062 | TLS | 720 | 1.4 | $R_C$ | 20.0 |
| 8.10.2005 | 0.074 | TLS | 720 | 1.6 | $V$ | 21.5 |
| 8-10.10.2005 | 0.819 | UVOT | 11474 | 2.5 | $uvw2$ | 23.2 |
| 8-10.10.2005 | 0.824 | UVOT | 10822 | 2.5 | $uvw1$ | 22.5 |
| 8-10.10.2005 | 0.845 | UVOT | 11887 | 2.5 | $uvm2$ | 22.7 |
| 8-10.10.2005 | 0.887 | UVOT | 11181 | 2.5 | $u$ | 22.5 |
| 10-14.10.2005 | 4.128 | UVOT | 125336 | 2.5 | $v$ | 22.8 |
| 27.10.2005 | 19.46 | TLS | 1800 | 1.7 | $I_C$ | 20.0 |
| 29.10.2005 | 21.47 | TLS | 5400 | 2.5 | $R_C$ | 22.7 |
| 28.04.2006 | 202.3 | ZTSh | 4260 | 1.9 | $R_C$ | 24.1 |
| 20.06.2006 | 255.3 | NOT | 4800 | 0.9 | $R$ | 25.7 |
| 30.06.2006 | 265.2 | NOT | 4800 | 1.2 | $V$ | 25.7 |
| 25.07.2006 | 290.1 | ZTSh | 2760 | 1.5 | $R_C$ | 23.5 |
| 12.08.2006 | 308.2 | NOT | 3300 | 0.7 | $B$ | 25.9 |
| 20.08.2006 | 316.2 | NOT | 4200 | 0.9 | $i$ | 22.5 |
| 16.09.2007 | 709.9 | AZT-22 | 12120 | 2.0 | $I_C$ | 22.5 |
| 12.02.2008 | 856.9 | Keck I | 780 | 0.85 | $R_C$ | 26.1 |
| 12.02.2008 | 856.9 | Keck I | 960 | 0.85 | $g'$ | 27.2 |
| 20.05.2009 | 1289.9 | NOT | 8400 | 1.1 | $i$ | 23.9 |
| 24.06.2010 | 1719.0 | Gemini | 1620 | 0.5 | $K'$ | 23.0 |
| 20.02.2012 | 2325.7 | Keck I | 930 | 1.8 | $B$ | 25.8 |
| 20.02.2012 | 2325.7 | Keck I | 810 | 1.8 | $I$ | 25.2 |
| 15.03.2012 | 2349.6 | Keck I | 930 | 1.1 | $U$ | 25.4 |
| 15.03.2012 | 2349.6 | Keck I | 720 | 1.1 | $Z$ | 25.5 |

**Table 5.** Photometric magnitudes (Vega) of the Id1–5 sources based on the observations made with the *Swift*/UVOT and TLS in October 2005, ZTSh in April 2006, the NOT in June–August 2006 and May 2009, Keck in 2008-2012 and Gemini in 2010. The magnitudes displayed in the table are in the Vega photometric system and have been dereddened for Galactic extinction (Schlegel, Finkbeiner & Davis 1998).

| Filter | Id1, $m$ | Id2, $m$ | **Id3, $\mathbf{m}$** | Id4, $m$ | Id5, $m$ | Instrument |
|---|---|---|---|---|---|---|
| $uvw2$ | 21.69 (0.18) | 22.29 (0.26) | $> \mathbf{23.3}$ | $> 23.3$ | $> 23.3$ | *Swift*/UVOT |
| $uvm2$ | 21.17 (0.16) | 22.66 (0.33) | $> \mathbf{22.8}$ | $> 22.8$ | $> 22.8$ | *Swift*/UVOT |
| $uvw1$ | 21.31 (0.19) | 22.30 (0.39) | $> \mathbf{22.6}$ | $> 22.6$ | $> 22.6$ | *Swift*/UVOT |
| $u$ | 21.32 (0.16) | $> 22.6$ | $> \mathbf{22.6}$ | $> 22.6$ | $> 22.6$ | *Swift*/UVOT |
| $U$ | 21.30 (0.04) | 22.92 (0.07) | **25.32 (0.23)** | 25.13 (0.19) | 25.46 (0.28) | Keck I/LRIS |
| $B$ | 21.80 (0.20) | 23.63 (0.21) | **25.20 (0.23)** | 25.28 (0.27) | 25.70 (0.26) | NOT/ALFOSC |
| $B$ | 22.12 (0.03) | 23.44 (0.07) | **25.27 (0.13)** | 25.22 (0.13) | 25.67 (0.19) | Keck I/LRIS |
| $g'$ | 21.77 (0.05) | 23.49 (0.07) | **24.57 (0.07)** | 24.94 (0.13) | 25.19 (0.19) | Keck I/LRIS |
| $v$ | 22.27 (0.29) | $> 22.8$ | $> \mathbf{22.8}$ | $> 22.8$ | $> 22.8$ | *Swift*/UVOT |
| $V$ | 21.50 (0.13) | 22.93 (0.14) | **24.45 (0.13)** | 24.75 (0.18) | 24.91 (0.19) | NOT/ALFOSC |
| $R$ | 21.15 (0.04) | 22.30 (0.09) | **24.07 (0.11)** | 24.16 (0.12) | 24.38 (0.11) | NOT/ALFOSC |
| $R$ | 21.35 (0.08) | 22.42 (0.13) | **24.01 (0.24)** | $> 24.1$ | $> 24.1$ | ZTSh |
| $R_C$ | 21.22 (0.05) | 22.39 (0.07) | **24.06 (0.10)** | 24.13 (0.13) | 24.33 (0.13) | Keck I/LRIS |
| $R_C$ | 21.18 (0.08) | 22.28 (0.26) | $> \mathbf{22.7}$ | $> 22.7$ | $> 22.7$ | TLS |
| $I$ | 20.23 (0.03) | 21.33 (0.02) | **23.88 (0.11)** | 23.90 (0.11) | 24.14 (0.14) | Keck I/LRIS |
| $i$ | 20.37 (0.05) | 21.53 (0.06) | **24.01 (0.15)** | 23.81 (0.17) | 23.98 (0.16) | NOT/ALFOSC |
| $Z$ | 20.29 (0.08) | 21.31 (0.09) | **23.80 (0.13)** | 23.78 (0.18) | 23.93 (0.18) | Keck I/LRIS |
| $K'$ | 18.49 (0.10) | 19.18 (0.11) | **22.86 (0.29)** | $> 23.0$ | $> 23.0$ | Gemini/NIRI |

**Table 6.** Reference stars used for the source photometry. The data are adopted from the SDSS-DR7 catalogue (Abazajian et al. 2009). The magnitudes are in the AB photometric system.

| Star's ID | RA, J2000 | Dec, J2000 | $u$ | $g$ | $r$ | $i$ | $z$ |
|---|---|---|---|---|---|---|---|
| J133138.56+420443.5 | 13 31 38.57 | +42 04 43.6 | 22.110 | 20.507 | 20.028 | 19.826 | 19.755 |
| J133137.89+420705.4 | 13 31 37.89 | +42 07 05.5 | 20.073 | 19.010 | 18.831 | 18.742 | 18.694 |
| J133141.93+420803.0 | 13 31 41.93 | +42 08 03.1 | 23.900 | 22.618 | 21.203 | 19.684 | 18.925 |
| J133146.39+420825.9 | 13 31 46.39 | +42 08 25.9 | 21.217 | 19.594 | 19.097 | 18.827 | 18.755 |
| J133145.90+420730.4 | 13 31 45.91 | +42 07 30.4 | 22.789 | 20.456 | 19.836 | 19.586 | 19.367 |
| J133133.58+420401.4 | 13 31 33.58 | +42 04 01.5 | 15.456 | 13.973 | 13.497 | 13.769 | 13.286 |
| J133153.54+420304.7 | 13 31 53.54 | +42 03 04.8 | 19.365 | 16.792 | 15.435 | 14.779 | 14.414 |

the best-fitted SED, the redshift, and the other required parameters. For all 5 galaxies we tried 3 different reddening laws: LMC (Fitzpatrick 1986), SMC (Prévot et al. 1984), and the reddening law for starburst galaxies (Calzetti et al. 2000). In case of the galaxy Id3 the best-fit is the LMC reddening law. The best-fit reddening laws for the galaxies Id1,2,4,5 are listed in Table 7. Figure 7a shows the best-fit SED of the galaxy Id3. It reveals that the burst occurred in a moderately absorbed LBG. It is one of the few cases where a LBG hosts a GRB (see also Odewahn et al. 1998; Jakobsson et al. 2005a; Malesani et al. 2013).

The redshift of $z = 2.77$ corresponds to a luminosity distance of 23.5 Gpc and a distance modulus of $46\overset{\mathrm{m}}{.}8$, one arcsecond corresponds to 8.0 proper kpc. For the galaxies Id3–Id5 the angular size is estimated as the full width at half maximum of the point spread function during the observations made on February 12, 2008 (see Table 7), which is equal to $0\overset{''}{.}9$.

It is worth noting that the galaxies Id1 and Id2 have redshifts of $z_{Id1} = 0.73^{+0.10}_{-0.08}$ and $z_{Id2} = 0.70^{+0.11}_{-0.08}$ (95% confidence level) with corresponding probability of $> 99.99\%$. These redshifts differ from those of the three other galaxies. This is a foreground group of at least two irregular interacting galaxies situated at a redshift of $z \sim 0.7$. SEDs of all studied galaxies except for Id3 are shown in Figure 7b.

Evans et al. (2009) used the spectrum of the GRB X-ray afterglow to determine the hydrogen column density along the line of sight in the host galaxy of GRB 051008: $N_H = (3.15 \pm 0.35) \times 10^{21}$ cm$^{-2}$ (the provided redshift of the absorber is equal to 0). We used the $N_H$–redshift-limit relation from Grupe et al. (2007) to estimate the upper limit of the GRB 051008 redshift to be $z < 2.8$. While the upper limit is consistent with our photo-$z$ estimate one can note that this method is based on a sample of unobscured bursts, and may be biased toward lower upper limits. It is known that for optically dark bursts $N_H$ values tend to be systematically higher (e.g., Fynbo et al. 2009; Krühler et al. 2012a; see also Table 10).

We estimate the star-formation rate (SFR) in the galaxy from its ultraviolet luminosity according to Kennicut (1998). Using the best fitted SED and the best host extinction law one can estimate the UV luminosity of Id3 to be $L_{UV} \sim 4.5 \times 10^{29}$ erg/s/Hz. For the SFR it gives an estimate of $\sim 60$ M$_\odot$/yr. The *LePhare* package with the PEGASE2 library also gives the best fitted values of the host physical parameters: star-formation rate SFR$_{PEGASE2} \sim 60$ M$_\odot$/yr and the stellar mass of the galaxy $M \sim 1.2 \times 10^9$ M$_\odot$.

In comparison with LBGs with $L^*$ luminosity Id3 is slightly under-luminous (by $\sim 0.5$ magnitudes in the rest-frame $V$-band) and has bluer colours. The age of the dominant stellar population of 60 Myr is 5 times less than the average value for LBGs, which is not unusual for LBGs: about 25% of LBGs have age $< 40$ Myr (Shapely et al. 2001). Also the Id3 galaxy is less dusty than an average LBG and 10 times less massive. Its SFR is less than the average LBG SFR, but close to it.

## 4 PROPERTIES OF GRB 051008 AND ITS AFTERGLOW

The X-ray afterglow data from *Swift*/XRT [14] provides the 2–10 keV flux for the time interval from 3070 to 445845 seconds after the burst onset. Eleven hours after the burst the X-ray flux was equal to $1.083 \times 10^{-12}$ erg/cm$^2$/s. The 3-keV spectral density of the X-ray flux at 11 hours after the trigger, converted in accordance with Jakobsson et al. (2004), is $F_X(3\text{ keV}, 11^h) = 0.018 \times 10^{-6}$ Jy. Assuming that the break at $\sim 0.41$ days (see Section 2.4) is the achromatic jet-break we extrapolated the optical upper limit of $23\overset{\mathrm{m}}{.}3$ toward 11 hours after the trigger using the XRT light curve. We estimate the optical flux to be $F_O(R, 11^h) < 0.068 \times 10^{-6}$ Jy. From this we derive $\beta_{OX}(11^h) \leqslant 0.02$, which allows us to classify this event as a dark burst. Since the spectral slope in X-ray regime is $\beta_X = 1.1$ (see the end of this Section), this burst is also dark according to the van der Horst et al. (2009) criterion.

We calculated the limit of the isotropic-equivalent radiated energy, using the redshift value, as $E_{iso} = (1.13 \pm 0.20) \times 10^{54}$ erg (in the energy range 20 keV – 10 MeV), and it is a lower estimate based on Konus-*WIND* measurements (see Section 2.2). Performing $k$-correction (e.g., Bloom et al. 2001) $E_{iso,\,corrected} = (1.15 \pm 0.20) \times 10^{54}$ erg. The collimated energy can be estimated given $E_{iso}$ and the opening angle of the jet. To calculate the jet opening angle of GRB 051008, we use the corresponding formula from Sari, Piran & Halpern (1999) and Liang et al. (2007), which relates this parameter to the isotropic-equivalent radiated energy $E_{iso}$ and the break time $t_b = 0.41^d$ of the afterglow light curve (see Section 2.4):

$$\theta_j \sim 0.161 \left(\frac{t_b}{1+z}\right)^{3/8} \left(\frac{E_{K,iso,52}}{n}\right)^{-1/8}. \quad (2)$$

Here $n$ is the constant ISM density, and $E_{K,iso,52}$ is the total isotropic kinetic energy of the outburst in the units of $10^{52}$ erg. The latter value is related to the isotropic-equivalent energy via a formula $E_{iso} = \xi E_{K,iso}$, where $\xi$ is the coefficient of conversion of the kinetic energy of the outburst into radiation energy, which depends on the ambient medium of the GRB source. We assume that the density of the medium and the conversion coefficient are equal to $n = 1$ and $\xi = 0.1$ (e.g., Zhang et al. 2007), respectively. Given the redshift, the break time of the light curve, and the equivalent isotropic energy, we estimate the jet opening angle as $\theta_{j,ISM} = 1^\circ.7 \pm 0^\circ.2$. Taking these values into account,

[14] http://www.swift.ac.uk/xrt_curves/00158855/flux.qdp

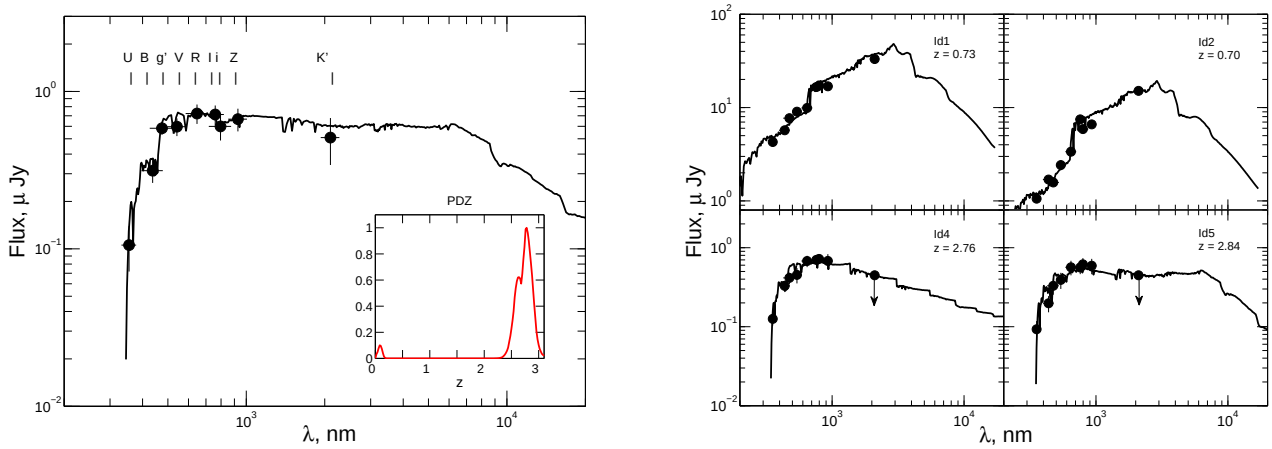


a) b)

**Figure 7. a)** Spectral Energy Distribution (SED) of the galaxy Id3 in the observer frame. The best-fitted SED type obtained by *Le Phare* (line) is the SED of a starburst galaxy. Observed flux in $UBg'VRiIZK'$ filters is shown by black circles. The associated Probability Distribution Function is shown in the inset. **b)** The best-fitted SEDs of the galaxies Id1, Id2, Id4 and Id5 obtained by *Le Phare* with observational data marked as in the figure a).

**Table 7.** parameters of the Id1–5 galaxies determined using *Le Phare*. Column 1 gives the galaxy ID; column 2 – the photometric redshift with 95% confidence level errors; column 3 – the corresponding probability; column 4 – corresponding $\chi^2$ per degree of freedom; column 5 – the most likely galaxy SED type (Im – irregular and interacting galaxies; B – starburst galaxies); column 6 gives the best fitted reddening law (LMC – the law for Large Magellanic Cloud Fitzpatrick 1986, SMC – the law for Small Magellanic Cloud Prévot et al. 1984, sb – the law for starburst galaxies Calzetti et al. 2000), column 7 – the age of the dominant stellar population of the galaxy in Gyr; column 8 – the internal extinction in the galaxy; column 9 – the R-band absolute magnitude of the galaxy, and column 10 gives the size of the galaxy in kpc.

| Id | $z \pm \Delta z$ | Probability, % | $\chi^2/DOF$ | Type of SED | Ext.law | Age, Gyr | $A_V$, mag | $M_R$, mag | d, kpc[a] |
|---|---|---|---|---|---|---|---|---|---|
| 1 | $0.73^{+0.10}_{-0.08}$ | $> 99.99$ | 46/13 | Im | sb | 0.50 | 0.28 | $-22.26$ | $49.7 \pm 1.4$ |
| 2 | $0.70^{+0.11}_{-0.08}$ | $> 99.99$ | 54/13 | Im | sb | 0.60 | 0.35 | $-21.23$ | $46.3 \pm 2.6$ |
| **3** | $\mathbf{2.77^{+0.15}_{-0.20}}$ | **96.32** | 4.0/9 | **B** | LMC | **0.06** | **0.31** | $\mathbf{-22.79}$ | $\mathbf{< 7.2}$ |
| 4 | $2.76^{+0.14}_{-0.12}$ | 99.98 | 4.8/9 | B | sb | 0.02 | 0.49 | $-21.60$ | $< 7.2$ |
| 5 | $2.84^{+0.16}_{-0.19}$ | 98.23 | 5.0/9 | B | LMC | 0.05 | 0.03 | $-22.30$ | $< 7.2$ |

the collimation-corrected gamma-ray energy can be estimated as $E_{\gamma,ISM} = (4.80 \pm 1.52) \times 10^{50}$ erg.

If the GRB progenitor is situated in a wind environment one can use equation (5) from Chevalier & Li (2000) which connects the jet opening angle $\theta$ and the parameters of the wind-like medium:

$$\gamma = 5.9 \left(\frac{1+z}{2}\right)^{1/4} E_{52}^{1/4} A_*^{-1/4} t_{b,days}^{-1/4}, \theta_j = 1/\gamma, \quad (3)$$

where $E_{52}$ is the isotropic-equivalent energy in units of $10^{52}$ erg, $t_{b,days}$ is the jet-break time in days, and $A_*$ is a parameter of the medium, related to the density profile as following: $n = Ar^{-2}$, and $A = A_* \times 5 \times 10^{35}$ cm$^{-1}$. Assuming $A_* = 1$ we can estimate the value of the jet opening angle $\theta_{j,wind} = 2^\circ.0 \pm 0^\circ.2$ and corresponding collimated gamma radiation energy $E_{\gamma,wind} = (7.20 \pm 1.54) \times 10^{50}$ erg.

Using the value of the peak energy in the burst spectrum, we can plot the parameters of GRB 051008 in the Amati diagram (Amati 2006). Data of 95 GRBs used for the Amati diagram (Fig. 8) were taken from Konus-*WIND* observations. Additionally, using $\theta_j$ one can put GRB 051008 in the Ghirlanda diagram (Ghirlanda et al. 2004), an empirical diagram showing the correlation between the peak energy in the spectrum and the emitted $\gamma$-ray energy, i.e., $E_{iso}$ corrected for the jet collimation (see Fig. 8). While the GRB fits well into the Amati correlation, it is evident that in case of an ISM environment, it does not agree with the Ghirlanda correlation. For the possible explanation see Section 5.1.

We extracted the X-ray spectrum from the raw *Swift*/XRT data using the XSPEC V12 software (a part of the HEAsoft software package[15]) for two different epochs: (a) $t - t_0 = 3072$ – 5393 seconds ($\sim$ 50 minutes after the trigger) and (b) $t - T_0 =$ 14806 – 17031 seconds (i.e. $\sim$ 4 hours after the trigger). The data were calibrated using the HEASARC CALibration Data Base (CALDB[16]) and fitted with single power-law with two absorption models (*phabs*zphabs*powerlaw*). The values of the Galactic absorption of $N_{H,Gal} = 1.05 \times 10^{20}$ cm$^{-2}$ and the redshift of $z = 2.77$ were fixed. The fitting provided the value of the host absorption at the assumed redshift of $N_{H,host}(a) = (7.7 \pm 1.2) \times 10^{22}$ cm$^{-2}$, $N_{H,host}(b) = (7.9 \pm 1.6) \times 10^{22}$ cm$^{-2}$ and the photon index $\Gamma(a) = 1.8 \pm 0.1$, $\Gamma(b) = 2.1 \pm 0.2$. The value of $N_{H,host}$ is

[15] http://heasarc.gsfc.nasa.gov/docs/software/lheasoft/
[16] http://heasarc.gsfc.nasa.gov/FTP/caldb

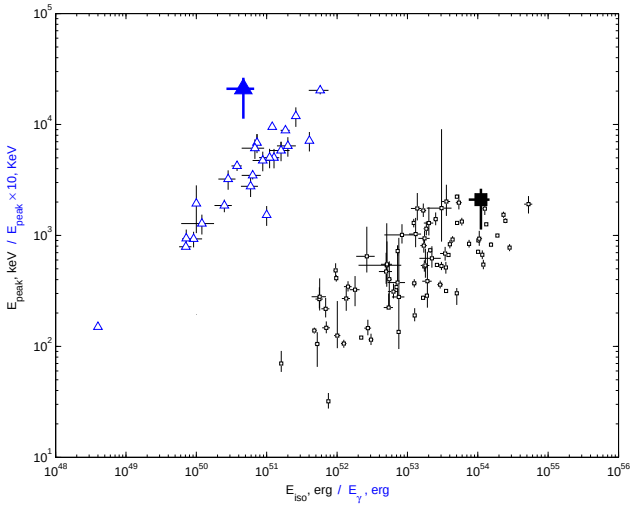


**Figure 8.** The Amati (squares, Amati 2006) and the Ghirlanda (triangles, Ghirlanda et al. 2004) diagrams. The Amati diagram displays the dependence of the energy corresponding to the maximum in the spectrum, $E_p(1+z)$, on the isotropic equivalent energy, $E_{iso}$. The Ghirlanda diagram displays the dependence of the energy $E_p(1+z)$ on the collimated energy , $E_\gamma$ (adapted from Ghirlanda et al. 2004). Filled symbols indicate the data points corresponding to GRB 051008, which can be seen to be in agreement with the Amati relation, but is a moderately significant outlier of the Ghirlanda relation assuming $z = 2.77$. The Ghirlanda diagram is shifted up along the Y axis by a factor of 10 for clarity.

**Table 8.** Summary of the properties of the host.

| | |
|---|---|
| RA | $13^h31^m29\overset{s}{.}510$ |
| Dec. | $+42°05'53\overset{''}{.}67$ |
| $z_{phot}$ | 2.77 (+0.15,-0.20) (95% confidence level) |
| SED type | starburst |
| $A_{V,bulk}$ | $\sim 0\overset{m}{.}31$ |
| $M_B$ | $-21\overset{m}{.}6 \pm 0\overset{m}{.}3$ |
| $M_R$ | $-22\overset{m}{.}8 \pm 0\overset{m}{.}1$ |
| $M_{K'}$ | $-23\overset{m}{.}9 \pm 0\overset{m}{.}3$ |
| Age | 60 Myr |
| Mass | $1.2 \times 10^9 M_\odot$ |
| SFR | $\sim 60 M_\odot$/y |

**Table 9.** Summary of the GRB and afterglow properties.

| | | |
|---|---|---|
| $N_{H,z}$ | $(7.9 \pm 1.6) \times 10^{22}$ cm$^{-2}$ | |
| $E_{iso}$ | $(1.15 \pm 0.20) \times 10^{54}$ erg | |
| $t_b$ | $0.41 \pm 0.14$ days | |
| $\alpha_1$ | $1.30 \pm 0.18$ | |
| $\alpha_2$ | $3.18 \pm 0.20$ | |
| $\beta_{OX}$ (11 hours) | $< 0.02$ | |
| $\beta_X$ (4 hours) | $1.1 \pm 0.2$ | |
| | ISM | wind |
| $\theta_j$ | $1°.7 \pm 0°.2$ | $2°.0 \pm 0°.2$ |
| $E_\gamma$ | $(4.80 \pm 1.52) \times 10^{50}$ erg | $(7.20 \pm 1.54) \times 10^{50}$ erg. |

one of the highest known, even for dark bursts (see Table 10). Using this data we can estimate the extinction along the line of sight to the GRB source. We construct the optical SED of the afterglow extrapolating the XRT spectral slope to the optical bandwidth with a cooling break in the soft end of the X-ray spectrum (the most conservative estimation). Next we apply the LMC extinction law in the host galaxy to the model of the SED (see Section 3). Then we normalize the model of the optical SED to the upper limit obtained in the same epoch using the early Shajn observation. The resulting value of the total extinction $A_V^{total}$ in the rest frame is 3 magnitudes (which effectively is a lower limit for the total extinction). The intrinsic extinction in the host galaxy is $A_V^{host} = 0\overset{m}{.}31$. This value may vary significantly depending on the specific sightline through the galaxy even if we assume a homogeneous distribution of the absorbing interstellar medium. For a conservative estimation we assume $A_V^{host} \sim 1^m$. Thus the source suffers from additional extinction along the line of sight $A_V^{LOS} > 2^m$. This indicates that there is an additional absorber in the line of site.

## 5 DISCUSSION

### 5.1 Properties of GRB 051008

We would like to emphasize several properties of GRB 051008. The absence of statistically significant spectral lag places the burst in the top 17% of the Konus-*WIND* burst sample and into the $\sim 10\%$ of long bursts without spectral lag in the BATSE (Hakkila et al. 2007) and *Swift* (Ukwatta et al. 2010) samples. The hardness of the burst, especially the high $E_{peak} = 770$ (CPL) keV of the main peak of the GRB, which corresponds to $\approx 2.9$ MeV in the rest frame and places the burst in the 7% of hardest time-resolved spectra of the BATSE sample (Kaneko et al. 2006).

GRB 051008 is clearly a long duration burst ($T_{90} = 214$ s as seen by Konus-*WIND* and $T_{90} = 535$ s as seen by SPI-ACS). The burst consists of a hard main peak and a somewhat softer tail detectable up to $\sim 800$ s. As we have seen from the joint BAT, SPI-ACS and XRT analysis the light curve can be described by a single power-law after the main peak of the burst up to the jet-break episode. The burst belongs to the less-frequent class of plateau-less X-ray afterglows (Liang et al. 2009).

From the modelling of the SED of the host galaxy one can conclude that GRB 051008 is optically dark neither because of high redshift ($z = 2.77$), nor due to the global absorption in the host galaxy $A_V = 0\overset{m}{.}31$. The lack of an OA is likely caused by absorption in the circumburst medium or by a dense cloud along the line of sight.

The burst is an outlier of the Ghirlanda relation assuming a value for the ISM density, $n = 1$. An option to make GRB 051008 agree with the Ghirlanda diagram is that the density of the ISM could be drastically higher, $n = 10^4 - 10^6$ instead of $n = 1$ used in our previous estimates. In case of a wind profile, we can estimate the necessary normalization in the density profile $A$ of $n = Ar^{-2}$ needed to fulfil the Ghirlanda relation. Let us assume $E_\gamma = 8.2 \times 10^{51}$ erg which would be needed to put GRB 051008 on the Ghirlanda relation. This yields the value of the jet opening angle to be $\theta \approx 7°$. Using equation (5) from Chevalier & Li (2000) we obtain the value of $A_* = 140$ cm$^{-1}$, and $A = A_* \times 5 \times 10^{35}$ cm$^{-1}$ $= 4.2 \times 10^{37}$ cm$^{-1}$. The normalization is $\sim 100$ times greater than the typical wind parameters of Wolf-Rayet stars (e.g., Castro-Tirado et al. 2010). This fact supports the hypothesis that the burst progenitor is embedded in a dense circumburst medium with a density of $n = 10^4 - 10^6$ cm$^{-3}$ rather than the absorber being along the line of sight.

If we suggest a high density of a circumburst medium, one might expect an appearance of a bright radio counterpart. E.g., for

GRB 111215A (Zauderer et al. 2013) the maximum of the radio afterglow light curve at 5.8 GHz was observed approximately 15 days after the burst at the level of about 1 mJy. Unfortunately, there were no long-term radio observations of GRB 051008 and deep upper limits (see Section 2.6) are not in contradiction with a possible radio afterglow evolution similar to that obtained for GRB 111215A by Zauderer et al. (2013).

Finally, the fact that the redshifts of two further galaxies (Ids 4, 5, Table 7) are close to $z_{Id3} = 2.77^{+0.15}_{-0.20}$ may support the hypothesis that the host galaxy could be gravitationally paired with at least one other galaxy at a projected distance of about 50 kpc. The distance between the galaxies Id3 and Id4 is $46 \pm 10$ kpc, if we adopt a common redshift of $z = 2.77$.

### 5.2 Comparison with other dark bursts

Table 10 lists the parameters of dark bursts for which host galaxies have been found. The table partially overlaps with the dark burst sample presented by Perley et al. (2013). Our table lists the following parameters of the galaxies: redshift, apparent and absolute $R$-band magnitudes, colour information, intrinsic host absorption, absorption along the line of sight to the GRB source, hydrogen column density, and star-formation rate. It comes as no surprise that the GRBs presented in Table 10 exhibit high line-of-sight extinction, since the assumption employed in selecting this sample (i.e., a redshift that does not point to the influence of Lyman absorption, and the application of a single synchrotron spectrum in modelling the broad-band SED) leave extinction as the strongest choice to explain the optical/NIR darkness (Krühler et al. 2012a; Perley et al. 2013). We also find that many dark-burst host galaxies exhibit a high SFR, with the median SFR for $z > 1$ hosts in our list being $\approx 40\ M_{\odot}$/yr. Indeed, GRB 051008 is one of the most distant bursts for which a host galaxy has been investigated in detail.

Greiner et al. (2011) analysed the extinction along the line of sight through (undetected) host galaxies of 33 GRBs, nine of which are dark bursts. The values of $A_V$ were obtained directly from observed SEDs of the afterglows (X-ray and optical). They found that a significant fraction of the bursts (25%) have $A_V \sim 0\overset{\mathrm{m}}{.}5$ and another 10% have $A_V > 1^m$. GRB 051008 with its $A_{V,LOS} > 2^m$ is located in the 10% of the bursts with high $A_V$ (Zafar et al. 2011).

### 5.3 Conclusions

In this paper we gathered almost all available observations of the dark GRB 051008, including $\gamma$-ray and X-ray data, optical imaging and spectroscopy, NIR, and radio data. GRB 051008 is clearly an optically dark burst. No OA was detected for GRB 051008 to a limit of $23\overset{\mathrm{m}}{.}3$ within half an hour after the burst trigger, and the burst is dark in accordance with the darkness criteria of both Jakobsson et al. (2004) and van der Horst et al. (2009). We detected and studied the host galaxy of GRB 051008. It is a rather typical Lyman-break galaxy located at the redshift of $z_{phot} = 2.77^{+0.15}_{-0.20}$. The host galaxy has a SFR of $\sim 60 M_{\odot}/$ yr typical for LBGs. The host is slightly younger and less dusty than LBGs with $L^*$ luminosity, and it is almost 10 times less massive. It is one of the few cases where a GRB host has been found to be a classical Lyman-break galaxy.

The redshift and the detection of GRB 051008 with Konus-*WIND* allowed us to calculate the isotropic-equivalent energy of the burst to be $E_{iso} = (1.15 \pm 0.20) \times 10^{54}$ erg. This is a highly energetic long burst without detectable spectral lag and with a hard spectrum and rather early jet-break of $\sim 0.41$ days determined from X-ray observations. The study of the host galaxy infers the presence of additional line of sight extinction towards the burst source. This extinction can not be explained by the bulk extinction in the host galaxy, which is only moderate. Most probably it is produced by a dense circumburst medium.

We furthermore found the photometric redshift of nearby galaxies, and among them the two galaxies have a redshift $z \sim 2.8$, coinciding with the redshift of the host within statistical uncertainties. Therefore, the host may be situated in a gravitationally bound system. The redshift of all three galaxies is determined due to the presence of a clear and strong Lyman break feature.

## ACKNOWLEDGMENTS

We are grateful to S.N. Dodonov, T.A. Fatkhullin, M.V. Barkov, O.V. Egorov, M. Salvato, D.I. Karasyov, and V.A. Kolesnikov for useful discussions. A.A.V., A.S.P. and P.Yu.M. were supported by the program "Origin, structure, and evolution of objects in the Universe" funded by the Russian Academy of Sciences and RFBR grants 12-02-01336-a, 13-01-92204-Mong, 14-02-10015-K.

J.G. and A.J.C-T. were supported by the Spanish programs ESP2005-07714-C03-03, AYA2007-63677, AYA2008-03467/ESP, and AYA2009-14000-C03-01. The data presented in this paper have been acquired using the ALFOSC camera, which is owned by the Instituto de Astrofísica de Andalucía (IAA) and operated at the Nordic Optical Telescope under the agreement between IAA and NBIfAFG of the Astronomical Observatory of Copenhagen. The Konus-*WIND* experiment is partially supported by a Russian Space Agency contract, RFBR grants 12-02-00032a and 13-02-12017 ofi-m.

D. A. K. and S. K. acknowledge financial support by DFG grants Kl 766/13-2 and Kl 766/16-1. D. A. K. acknowledges financial support by MPE and TLS.

Support for D.A.P. is provided by NASA through Hubble Fellowship grant HST-HF-51296.01-A awarded by the Space Telescope Science Institute, which is operated for NASA by the Association of Universities for Research in Astronomy, Inc., under contract NAS 5-26555.

## REFERENCES

Abazajian K.N., Adelman-McCarthy J.K., Agueros M.A., et al., 2009, ApJ Supl.Series 182, 543
Amati L., 2006, MNRAS, 372, 233
Aptekar R.L., Frederiks D.D., Golenetskii S.V., et al., 1995, Space Sci.Rev., 71, 265
Arnaud K.A., 1996, in ASP Conf. Ser. 101, Astronomical Data Analysis Software and Systems V, ed. G. Jacoby, & J. Barnes, (San Francisco: ASP), 17
Arnouts S., Cristiani S., Moscardini L., et al., 1999, MNRAS, 310, 540
Band D.L., 1997, ApJ, 486, 928
Band D., Matteson J., Ford L., et al., 1993, ApJ, 413, 281
Beloborodov A.M., Stern B.E., Svensson R., 2000, ApJ, 535, 158
Beuermann K., Hessman F.V., Reinsch K., et al., A&A, 352, L26
Bloom J.S., Frail A.D., Sari R., 2001, AJ 121, 2879
Bloom J.S., Kulkarni S.R., Djorgovski S.G., 2002, AJ, 123, 1111
Bloom J.S., Berger E., Kulkarni S.R., et al., 2003, AJ, 125, 999
Bloom J.S., Prochaska J.X., Pooley D., et al., 2006, ApJ, 638, 354

**Table 10.** A comparison of the parameters of host galaxies of dark GRBs. Column 1 lists the name of the burst associated with the galaxy; Columns 2–4 indicate whether the burst had any X-ray, optical/NIR, or radio afterglow ("IR" means the detection of the OA only in the infrared domain, "n" means that no observations were made in the wavelength interval considered); Column 5 gives the spectral index ($^x$ – the spectral index $\beta_X - 0.5$ is adopted according to the van der Horst et al. 2009 darkness criterion); Column 6 lists the redshift (superscript $^p$ indicates that the redshift was determined photometrically); Column 7 gives the $R$ magnitude of the host galaxy; Column 8 presents the data on the colour of the galaxy; Column 9 gives internal bulk extinction in the galaxy; Column 10 – the extinction towards the GRB source along the line of sight; Column 11 – the hydrogen column density; Column 12 – the absolute $R$-band magnitude of the galaxy; Column 13 – the star-formation rate, and Column 14 – references: 1 – Djorgovski et al. (2001), 2 – Bloom et al. (2003), 3 – Gorosabel et al. (2003), 4 – Piro et al. (2002), 5 – Frail et al. (2003), 6 – Jakobsson et al. (2005b), 7 – Küpcü Yoldaş et al. (2010), 8 – Levan et al. (2006), 9 – Perley et al. (2013), 10 – Castro-Tirado et al. (2007), 11 – Perley et al. (2009), 12 – Tanvir et al. (2008), 13 – Jaunsen et al. (2008), 14 – Elíasdóttir et al. (2009), 15 – Svensson et al. (2012), 16 – Krühler et al. (2012a), 17 – Hunt et al. (2011), 18 – Hashimoto et al. (2010), 19 – Krühler et al. (2011), 20 – Krühler et al. (2012b), 21 – Chen et al. (2010), 22 – Holland et al. (2010), 23 – Greiner et al. (2013), $*$ refers to the present paper.

| GRB | X | O | R | $\beta_{OX}$ | $z$ | $R_{host}$ mag | Color mag | $A_{V,host}$ mag | $A_{V,LOS}$ mag | $N_H \times 10^{21}$, cm$^{-2}$ | M$_R$,$^m$ mag | SFR, $M_\odot$/yr | Reference |
|---|---|---|---|---|---|---|---|---|---|---|---|---|---|
| 970828 | + | − | + | 0.09 | 0.96 | 25.2 | $R-K=3.7$ | — | $>3.8$ | $>6$ | $-19.6$ | $\sim 1.2$ | (1) |
| 990506 | + | − | + | $<0.06$ | 1.31 | 24.3 | $(R-K)_{AB}=2.3$ | $>1$ | — | — | $-20.5$ | 12.6 | (2) |
| 000210 | + | − | + | 0.44 | 0.85 | 25.0 | $R-K=2.5$<br>$V-I\sim 1.7$ | $\sim 0$ | — | $5\pm1$ | $-22.2$ | $\sim 2.1$ | (3,4,5) |
| 020819 | n | − | + | — | 0.41 | 23.46 | $R-K=2.7$ | $1.8-2.6$ | $4-20$ | — | $-22.3$ | $<40$ | (6,7) |
| 030115 | + | + | + | — | $2.5-2.7^p$ | $25.58^a$ | $R-K=5.35$ | $\sim 1.0$ | — | — | — | $4.4-500$ | (8) |
| 050915A | + | − | n | 0.23 | 2.53 | 24.56 | $R-K=3.9$ | 1.0 | $\sim 1.4$ | $0.9^{+0.8}_{-0.7}$ | $-22.1$ | $135.8^{+63.1}_{-48.3}$ | (9) |
| 051008 | + | − | − | $<0.02$ | $2.77^p$ | 24.06 | $V-I=0.6$<br>$R-K=1.4$ | 0.31 | $>2$ | $79\pm16$ | $-22.8$ | $\sim 60$ | (*) |
| 051022 | + | − | + | $<-0.11$ | 0.81 | 21.5 | $R-K=3.3$<br>$V-I\sim 1.1$ | 1.0 | $>9$ | $34.7^{+4.8}_{-4.7}$ | $-21.8$ | $\sim 50$ | (9,10) |
| 060202 | + | − | n | $<0.20$ | 0.78 | $23.79^b$ | $(R-K)_{AB}=1.1$ | $\sim 1$ | 2.9 | $4.5^{+0.7}_{-0.6}$ | $-19.6$ | $5.8^{+1.3}_{-1.9}$ | (9) |
| 060210 | + | + | − | 0.37 | 3.91 | $24.33^b$ | $(R-I)_{AB}\approx 0.1$ | 0.25 | $1.2^{+0.2}_{-0.1}$ | $24.6^{+2.9}_{-3.5}$ | $<-20.2$ | $-23.4$ | (11) |
| 060306 | + | − | n | $<0.21$ | 1.55 | $24.49^b$ | $(R-K)_{AB}=2.5$ | $2.2\pm0.1$ | 4.6 | $3.0^{+0.8}_{-0.7}$ | $-20.8$ | $244^{+129}_{-67}$ | (9) |
| 060319 | + | + | n | 0.19 | 1.17 | $24.20^b$ | $(R-K)_{AB}=2.4$ | $0.1^{+0.2}_{-0.1}$ | 1.1 | $3.4^{+0.8}_{-0.7}$ | $-20.3$ | $0.0^{+0.4}_{-0.0}$ | (9) |
| 060719 | + | + | − | $-0.27$ | 1.53 | $24.62^b$ | $(R-K)_{AB}=1.8$ | $0.4^{+1.1}_{-0.4}$ | 2.1 | $3.4^{+1.3}_{-1.0}$ | $-20.6$ | $4.0^{+36.9}_{-4.0}$ | (9) |
| 060814 | + | + | n | $-0.21$ | 1.92 | 22.85 | $(R-K)_{AB}=1.2$ | $1.2^{+0.1}_{-0.0}$ | 3.1 | $2.7^{+0.4}_{-0.3}$ | $-23.0$ | $236.7^{+28.4}_{-18.3}$ | (9) |
| 060923A | + | + | − | 0.38 | $<2.8^p$ | 25.65 | $R-K\sim 4$<br>$V-I\sim 1.5$ | — | 2.6 | — | $<-21.2$ | — | (11,12) |
| 061222A | + | $+^{IR}$ | + | $<-0.19$ | 2.09 | 24.93 | $(V-I)_{AB}\sim 0.5$<br>$(I-K)_{AB}<1.0$ | $<0.5$ | $>5.0$ | $44.8^{+5.4}_{-3.0}$ | $-21.2$ | — | (9,11) |
| 070306 | + | $+^{IR}$ | − | 0.33 | 1.50 | $\sim 23$ | $R-K\sim 1.5$ | $\leqslant 0.45$ | $5.5\pm0.6$ | $26.8^{+4.7}_{-4.3}$ | $-22.2$ | $\sim 7.3$ | (13) |
| 070521 | + | − | n | $<-0.10$ | 1.35 | 26.11 | $V-I=0.72$ | — | $>9$ | $54^{+13}_{-11}$ | $-18.8$ | — | (11) |
| 070802 | + | + | n | 0.46 | 2.45 | 25.03 | $R-K\sim 3.3$ | $<1.5$ | $<0.3$ | $3.2\pm1.8$ | $-21.0$ | — | (14) |
| 071021 | + | $+^{IR}$ | + | 0.37 | 2.45 | $25.22^b$ | $(R-K)_{AB}=3.1$ | $1.6\pm0.3$ | 0.5 | $0.5^{+0.8}_{-0.5}$ | $-21.3$ | $108^{+98}_{-55}$ | (9) |
| 080207 | + | − | n | $<0.3$ | 2.08 | $>25.65$ | $R-K>5.4$ | $\sim 1.9$ | $\leqslant 3.4$ | $151^{+23}_{-22}$ | $>-19.9$ | $\sim 40$ | (15,16) |
| | | | | | $\sim 2.2^p$ | $\sim 25.8$ | $R-K\sim 6.3$ | $1-2$ | — | | | $\sim 119$ | (17) |
| 080325 | + | $+^{IR}$ | n | $0.14-0.33$ | 1.78 | 25.5 | $R-K_s=3.8$ | 0.8 | $2.7-10$ | $18^{+8}_{-6}$ | $-20.3$ | $10-80$ | (18,9) |
| 080605 | + | + | n | $0.17^x$ | 1.64 | 21.6 | $(R-K)_{AB}=0.5$ | $0.5\pm0.1$ | $1.2\pm0.1$ | $9.0\pm0.9$ | $-22.4$ | $49^{+26}_{-13}$ | (19,20) |
| 080607 | + | + | n | $0.14-0.37$ | 3.04 | $26.33^b$ | $(R-K)_{AB}=2.5$ | 1.25 | 3.3 | $1.4\pm0.4$ | $-20.8$ | $18.3^{+5.0}_{-3.2}$ | (9,21) |
| 081109A | + | + | − | $<0.44$ | 0.97 | 22.65 | $(R-K)_{AB}=1.6$ | $1.0\pm0.2$ | $3.4^{+0.4}_{-0.3}$ | $9\pm2$ | $-21.4$ | $33^{+19}_{-13}$ | (19) |
| 081221 | + | + | + | 0.00 | 2.26 | $24.67^b$ | $(R-K)_{AB}=2.5$ | $1.4\pm0.1$ | 1.4 | $3.9^{+0.5}_{-0.4}$ | $-21.6$ | $73^{+16}_{-13}$ | (9) |
| 090404 | + | − | + | $<0.20$ | $3.0^p$ | $26.07^b$ | $(R-K)_{AB}=3.1$ | $1.3^{+2.2}_{-1.2}$ | 1.3 | $5.1^{+1.0}_{-0.9}$ | $-21.0$ | $40^{+178}_{-22}$ | (9) |
| 090407 | + | − | n | $<0.14$ | 1.45 | $25.78^b$ | $(R-K)_{AB}=3.3$ | $1.8^{+0.1}_{-1.2}$ | 1.6 | $2.3\pm0.4$ | $-19.3$ | $16.6^{+1.8}_{-15.2}$ | (9) |
| 090417B | + | − | − | $<0.28$ | 0.34 | 21.34 | $R-K=2.8$ | $0.9\pm0.1$ | 2.7 | $8.3^{+1.4}_{-1.2}$ | $-20.0$ | $0.5\pm0.3$ | (9,22) |
| 090709A | + | − | − | $-0.56$ | $1.8^p$ | $26.39^b$ | $(R-K)_{AB}=2.7$ | $1.4^{+0.1}_{-0.2}$ | 3.0 | $1.7\pm0.3$ | $-19.3$ | $8.3^{+4.4}_{-3.6}$ | (9) |
| 090926B | + | + | n | $0.23^x$ | 1.24 | 22.94 | $(R-K)_{AB}=1.5$ | $1.4\pm0.3$ | $1.4^{+1.1}_{-0.6}$ | $13.9^{+1.6}_{-1.5}$ | $-21.8$ | $80^{+110}_{-50}$ | (19) |
| 100621A | + | + | n | 0.39 | 0.542 | 21.53 | $(R-K)_{AB}=0.3$ | $0.6\pm0.1$ | $3.8\pm0.2$ | $18.0^{+1.2}_{-1.1}$ | $-20.9$ | $13^{+6}_{-5}$ | (19,23) |

$^a$ in $F606W$ filter.
$^b$ synthetic AB magnitude.


Breeveld A., Marshall F., Blustin A., 2005, GCN Circ. No.4079
Burrows D.N., Hill J.E., Nousek J.A., 2005, Space Sci.Rev., 120, 165
Butler N.R., 2007, AJ, 133, 1027
Calzetti D., Armus L., Bohlin R.C., et al., 2000, ApJ, 533, 682
Cameron P.B., 2005, GCN Circ. No.4074
Castro-Tirado A.J., Bermer M., McBreen S., et al., 2007, A&A, 475, 101
Castro-Tirado A.J., Moller P., Garcia-Segura G., et al., 2010, A&A, 517, A61
Cenko S.B., Kelemen J., Harrison F.A., et al., 2009, ApJ, 693, 1484
Chandra P., Frail D.A., 2012, ApJ, 746, 156
Chen H.-W., Perley D.A., Wilson C.D., et al., 2010, ApJL, 723, L218
Chen H.-W., 2012, MNRAS, 419, 3039
Chevalier R.A., Li Z.-Y., 2000, ApJ 536, 195
Clocchiatti A., Suntzeff N.B., Covarrubias R., Candia P., 2011, AJ, 141, 163
Devyatkin A.V., Gorshanov D.L., Kouprianov V.V., Verestchagina I.A., 2010, Solar System Research 44, 68
Djorgovski S.G., Frail D.A., Kulkarni S.R., et al., 2001, ApJ, 562, 654
Elíasdóttir Á., Fynbo J.P.U., Hjorth J., et al., 2009, ApJ, 697, 1725
Evans P.A., Beardmore A.P., Page K.L., et al., 2009, Mon.Not.Roy.Astron.Soc. 397, 1177
Evans P.A., Willingale R., Osborne J.P., et al., 2010, A&A, 519, A102
Ferrero P., Klose S., 2005, GCN Circ. No.4076
Ferrero P., Klose S., Kann A., et al., 2005, GCN Circ. No.4085

Fioc M., Rocca-Volmerange B., 1997, A&A 326, 950
Fitzpatrick E.L., 1986, AJ, 92, 1068
Foley S., McGlynn S., Hanlon L., et al., 2008, A&A, 484, 143
Frail D.A., Kulkarni S.R., Berger E., Wieringa M.H., 2003, AJ, 125, 2299
Franx M., Labbé I., Rudnick G., et al., 2003, ApJ, 587, L79
Fynbo J.U., Jensen B.L., Gorosabel J., et al., 2001, A&A, 369, 373
Fynbo J.P.U., Jakobsson P., Möller P., et al., 2003, A&A, 406, L63
Fynbo J.P.U., Prochaska J.X., Sommer-Larsen J., et al., 2008, ApJ, 683, 321
Fynbo J.P.U., Jakobsson P., Prochaska J.X., et al., 2009, ApJS, 185, 526
Galama T. and Wijers R.A.M., 2001, ApJ, 549, L209
Gehrels N., Chincarini G., Giommi P., et al., 2004, ApJ, 611, 1005
Ghirlanda G., Ghisellini G., Lazzati D., 2004, ApJ, 616, 331
Goad M.R., Tyler L.G., Beardmore A.P., et al., 2007, A&A, 476, 1401
Gorosabel J., Christensen L., Hjorth J., et. al., 2003, A&A, 400, 127
Greiner J., Krühler T., Fynbo J.P.U. et al., 2009, 639, 1610
Greiner J., Krühler T., Klose S., et al., 2011, A&A, 526, A30
Greiner J., Krühler T., Nardini M., et al., 2013, A&A, 560, A70
Grupe D., Nousek J.A., vanden Berk D.E., et al., 2007, AJ 133, 2216
Hakkila J., Giblin T.W., Young K.G., et al., 2007, ApJS 169, 62
Hashimoto T., Ohta K., Aoki K., et al., 2010, ApJ, 719, 378
Holland S.T., Sbarufatti B., Sher R., et al., 2010, ApJ, 717, 223
Hughes. D. H., Serjeant S., Dunlop J., et al., 1998, Nature, 394, 241
Hunt L., Palazzi E., Rossi A., et al., 2011, ApJ Lett., 736, L36
Ilbert O., Arnouts S., McCracken H.J., et al., 2006, A&A, 457, 841
Jakobsson P., Hjorth J., Fynbo J. P. U., et al., 2004, ApJ, 617, L21
Jakobsson P., Bjrnsson G., Fynbo J.P.U., et al., 2005, MNRAS, 362, 245
Jakobsson P., Frail D.A., Fox D.B., et al., 2005, ApJ, 629, 45
Jakobsson P., Hjorth J., Malesani D., et al., 2012, ApJ, 752, 62
Jaunsen A.O., Rol E., Watson D.J., et al., 2008, ApJ, 681, 453
Jimenez R., Piran T., 2013, ApJ, 773, id. 126
Kaneko Y., Preece R.D., Briggs M.S., et al., 2006, ApJ,Supl. 166, 298
Kennicutt R.C., 1998, Ann.Rev.A&A, 36, 189
von Kienlin A., Beckmann V., Rau A., et al., 2003, A&A, 411, L299
Klose S., Hoegner C., 2005, GCN Circ. No.4072
Krühler T., Greiner J., Schady P., et al., 2011, A&A, 534, A108
Krühler T., Malesani D., Milvang-Jensen B., et al., 2012, ApJ, 758, 46
Krühler T., Fynbo J.P.U., Geier S., et al., 2012, A&A, id.A8
Küpcü Yoldaş A., Greiner J., et al., 2010, A&A, 515, L2
Lamb D.Q. and Reichart D.E., 2000, ApJ, 536, 1
Lazzati D., Covino S., Ghisellini G., 2002, MNRAS, 330, 583
Levan A., Fruchter A., Rhoads J., et al., 2006, ApJ, 647, 471
Liang E.-W., Racusin J.L., Zhang B., et al., 2008, ApJ, 675, 528
Liang E.-W., Lü H.-J., Hou S.-J., et al., 2009, ApJ, 707, 328
Malesani D., Kruehler T., Perley D., et al., 2013, GCN Circ. No.14225.
Margutti R., Zaninoni E., Bernardini M.G., et al., 2013, MNRAS, 428, 729
Marshall F., Barthelmy S., Cummings J., et al., 2005, GCN Circ. No.4069
Mazets E.P., Aptekar R.L., Butterworth P.S., et al., 2001, Gamma-Ray Bursts in the Afterglow Era: Proceedings of the International Workshop Held in Rome, Italy, 17-20 October 2000, ESO ASTROPHYSICS SYMPOSIA. ISBN 3-540-42771-6. Edited by E. Costa, F. Frontera, and J. Hjorth. Springer-Verlag, p. 9
Melandri, A., Mundell, C. G., Kobayashi, S., et al. 2008, ApJ, 686, 1209
Melandri A., Sbarufatti B., D'Avanzo P., et al., 2012, MNRAS 421, 1265
Minaev P., Pozanenko A., Grebenev S., Molkov, S., 2013, EAS Publications Series, 61, 75
Minaev P., Pozanenko A., Grebenev S., Molkov S., 2014, Astronomy Letters, 40, 271
Moretti A., Perri M., Capalbi M., et al., 2006, A&A, 448, L9
Moustakas L. A., Casertano S., Conselice C. J., et al., 2004, ApJ, 600, L131
Norris J.P., Marani G.F., Bonnell J.T., 2000, ApJ, 534, 248
Nousek J.A., Kouveliotou C., Grupe D., et al., 2006, ApJ, 642, 389
Odewahn S.C., Djorgovski S.G., Kulkarni S.R., et al., 1998, ApJ, 509, L5
Ohno M., Takahashi T., Fukazawa Y., et al., 2005, GCN Circ. No.4297
Oke J.B., Cohen J.G., Carr M., et al., 1995, Publ.Astron.Soc.Pacific 107, 375
Paczynski B., 1998, ApJ, 494, L45
Pelangeon A., Atteia J-L., 2005, GCN Circ. No.4086
Pérez-Ramírez D., de Ugarte Postigo A., Gorosabel J., et al., 2010, A&A, 510, 105
Perley D.A., Cenko S.B., Bloom J.S., et al., 2009, AJ, 138, 1690
Perley D.A., Morgan A.N., Updike A., et al., 2011, AJ, 141, 36
Perley D.A., Levan A. J., Tanvir N. R., et al., 2013, ApJ 778, id. 128
Perley D.A., Perley R.A., 2013, ApJ, 778, id. 172
Perri M., Capalbi M., Burrows D.N., 2005a, GCN Circ. No.4071
Perri M., Capalbi M., Burrows D.N., 2005b, GCN Circ. No.4073
Piro L., Frail D.A., Gorosabel J., et al., 2002, ApJ, 577, 680
Porciani C., Madau P., 2001, ApJ, 548, 522
Pozanenko A.S., Loznikov V.M., 2000, in Kippen R.M., Mallozzi R.S., Fishman G.J., eds., "Gamma-ray Bursts, 5th Huntsville Symposium", American Institute of Physics Conference Series, 526, 220
Pozanenko A., Rumyancev V., Ibrahimov M., et al., 2007, Izvestiya Crymskoi Astrof. Obs. 103, 48
Prévot M.L., Lequeux J., Prévot L., et al., 1984, A&A, 132, 389
Racusin J.L., Liang E.W., Burrows D.N., et al., 2009, ApJ, 698, 43
Rhoads J.E., 1997, ApJ Lett., 487, L1
Roming P.W.A., Kennedy T.E., Mason K.O., et al., 2005, Space Science Reviews, 120, 95
Roming P., Marshall F., Blustin A., 2005, GCN Circ. No.4070
Rossi A., Klose S., Ferrero P., et al., 2012, A&A, 545, A77
Rumyantsev V., Biryukov V., Pozanenko A., 2005, GCN Circ. No.4081
Sari R., Piran T., Narayan R., 1998, ApJ, 497, L17
Sari R., Piran T., Halpern J.P., 1999, ApJ, 519, L17
Savaglio S., Glazebrook K., Le Borgne D., 2009, ApJ, 691, 182
Schlegel D.J., Finkbeiner D.P., Davis M., 1998, ApJ, 500, 525
Shapely A.E., Steidel C.C., Adelberger K.L., et al., 2001, ApJ, 562, 95
Svensson K.M., Levan A.J., Tanvir N.R., et al., 2012, MNRAS, 421, 25

Tanvir N.R., Levan A.J., Rol E., et al., 2008, MNRAS, 388, 1743
Taylor G.B., Frail D.A., Kulkarni S.R., et al., 1998, ApJ, 502, L115
Tinney C., Stathakis R., Cannon R., Galama T.J., 1998, IAU Circ. 6896
Thöne C.C., Campana S., Lazzati D., et al., 2011, MNRAS, 414, 479
Thöne C.C., Fynbo J.P.U., Goldoni P., et al., 2013, MNRAS, 428, 3590
Turner E.L., Ostriker J.P., Gott, III, J.R., 1984, ApJ, 284, 1
van der Horst A.J., Kouveliotou C., Gehrels N., et al., 2009, ApJ, 699, 1087
Volnova A.A., Pozanenko A.S., Rumyantsev V.V., et al., 2010a, Astrophys.Bull., 65, 334
Volnova A.A., Pozanenko A.S., Rumyantsev V.V., et al., 2010b, in McEnery J.E., Racusin J.L., Gehrels N., eds., "Gamma Ray Bursts 2010" (Annapolis, MD, USA, 1-4 November 2010) AIP Conference Proceedings 1358, Greenbelt.
Ukwatta T.N., Stamatikos M., Dhuga K.S., et al., 2010, ApJ, 711, 1073
Ulanov M.V., Golenetskii S.V., Frederiks D.D., et al., 2005, Nuovo Cimento C, 28, 351
Wang J., Wei J.-Y., 2010, Res.Astron.Aph., 10, 533
Wright E.L., 2006, Publ.Astron.Soc.Pacific 118, 1711
Wyithe J.S.B., Oh S.P., Pindor B., 2011, MNRAS, 414, 209
Xin L.P., Zheng W.K., Wang J., et al., 2010, MNRAS, 401, 2005
Zafar T., Watson D., Fynbo J.P.U., et al., A&A, 532, id. A143
Zauderer B.A., Berger E., Margutti R., et al., 2013, ApJ, 767, 161
Zeh A., Klose S., Hartmann D.H., 2004, ApJ, 609, 952
Zhang B., Fan Y.Z., Dyks J., et al., 2006, ApJ, 642, 354
Zhang B., Liang E., Page K.L., et al., 2007, ApJ, 655, 989
Zheng W.-K., Deng J.-S., Wang J., 2009, Research in A&A, 9, 1103